metabolites

MDPI

Article

Integrated Plasma and Cerebrospinal Fluid Lipid Scores and Longitudinal Postural Instability and Gait Difficulty in Parkinson's Disease

Yinuo Qu [1,†], Yirui Chen [2,3,†], Hongxin Gui [2], Xiangyu Li [2], Xinyu Wang [2], Weichen Zhu [2], Zhuoya Wang [2], Zimu Wu [4], Mengyang Wang [2,*] and Tianrui Wang [5,6,*]

1 Affiliated Hospital of Shandong University of Traditional Chinese Medicine, Jinan 250355, China; noey1207@163.com
2 School of Public Health and Health Sciences, Tianjin University of Traditional Chinese Medicine, No. 10 Poyanghu Road, Jinghai District, Tianjin 301617, China; ciandata@163.com (Y.C.); ghostcixi@163.com (H.G.); lixiangyu0925888@163.com (X.L.); wangxinyu8218@163.com (X.W.); 16602288382@163.com (W.Z.); wzy2008011@126.com (Z.W.)
3 Department of Electronics, Information and Bioengineering (DEIB), Politecnico di Milano, Piazza Leonardo da Vinci 32, 20133 Milan, Italy
4 Centre for Epidemiology and Biostatistics, Melbourne School of Population and Global Health, University of Melbourne, Melbourne, VIC 3010, Australia; zimu.wu1@monash.edu
5 Modern Industrial College of Traditional Chinese Medicine Pharmaceutical Engineering, Tianjin University of Traditional Chinese Medicine, Tianjin 301617, China
6 Department of State-Owned Assets and Laboratory Management, Tianjin University of Traditional Chinese Medicine, Tianjin 301617, China
* Correspondence: mengyangwang@tjutcm.edu.cn (M.W.); wtr@tjutcm.edu.cn (T.W.)
† These authors contributed equally to this work.

Highlights

What are the main findings?

- Integrated lipid scores were associated with faster PIGD change in reference longitudinal models.
- Separate brain and donor-level astrocyte analyses identified reduced fatty-acid pathway expression in PD.

What are the implications of the main findings?

- The 16-lipid panel brings endolysosomal and membrane lipid biology into the study of a defined progression phenotype.
- Paired biofluid comparisons provide a basis for testing compartment-specific contributions in independent longitudinal cohorts.

Abstract

Background/Objectives: Gait and postural deterioration contribute to heterogeneous progression in Parkinson's disease (PD). Defining their metabolic correlates could guide biological stratification. We examined paired plasma and cerebrospinal fluid (CSF) lipid profiles in relation to longitudinal postural instability and gait difficulty (PIGD). **Methods:** This exploratory secondary Parkinson's Progression Markers Initiative analysis combined 16 bis(monoacylglycerol) phosphate, ceramide, and plasmalogen features into interpretable scores. Standardization used 213 participants with paired measurements. Longitudinal analyses included 193 participants, 1152 observations, and median follow-up of 5.17 years. Mixed-effects models assessed score-by-time associations, with clinical adjustment, matrix-specific comparisons, and participant-bootstrap inference. Separate brain- and donor-level astrocyte transcriptomes characterized lipid-related pathways. **Results:** A higher equal-analyte score was associated with faster PIGD change (0.01248 units/year per SD; model-

Check for updates

Academic Editor: Carlos Alberto Gonçalves

Received: 26 October 2026
Revised: 12 November 2026
Accepted: 19 November 2026
Published: 25 November 2026

Copyright: © 2026 by the authors. Licensee MDPI, Basel, Switzerland. This article is an open access article distributed under the terms and conditions of the Creative Commons Attribution (CC BY) license.

based 95% CI, 0.00447–0.02048; five-score q = 0.00563), corresponding to a five-year contrast of 0.0624 on the 0–4 scale. Clinical adjustment yielded a similar estimate (0.01408; 95% CI, 0.00646–0.02170; 162 participants). Participant-bootstrap intervals included zero. Class-balanced and matrix-specific scores also had positive estimates. Separate transcriptomic analyses identified reduced fatty-acid pathway expression in PD brain tissue and astrocytes. **Conclusions:** The defined lipid panel connects endolysosomal and membrane biology with axial motor trajectories and offers a focused target for longitudinal replication. Prospective evaluation could determine its value for biological stratification, trial enrichment, and the development of a practical plasma-based assessment strategy. Paired-compartment comparisons provide a basis for evaluating whether CSF contributes information beyond plasma measurements and established clinical measures.

Keywords: Parkinson's disease; lipid metabolism; plasma; cerebrospinal fluid; postural instability and gait difficulty; longitudinal analysis; astrocytes

1. Introduction

Parkinson's disease (PD) progresses at markedly different rates across individuals, complicating prognosis and clinical-trial design [1–3]. This heterogeneity also concerns the clinical domains through which progression becomes apparent. A molecular measure associated with a specific longitudinal domain could improve biological characterization of that variation.

Postural instability and gait difficulty (PIGD) provides a focused clinical domain for this investigation. Its constituent Movement Disorder Society–Unified Parkinson's Disease Rating Scale (MDS-UPDRS) items capture gait, freezing, and postural impairment [4]. Imaging and longitudinal studies implicate several contributors to axial deterioration [5–8]. The continuous five-item PIGD mean permits these features to be examined together over time.

Lipid biology offers a rationale for examining molecular differences associated with these trajectories. Lewy pathology contains membrane and organellar material, and human lipidomic studies report widespread glycerophospholipid and sphingolipid abnormalities [9,10]. These observations connect lipid metabolism with the cellular setting of PD. Their clinical relevance can be explored by relating defined lipid measurements to subsequent change in an axial motor composite.

Three lipid classes informed the present panel because they represent complementary aspects of membrane biology. Bis(monoacylglycerol) phosphate (BMP) participates in endolysosomal lipid handling, and urinary BMP varies with LRRK2 and GBA1 status [11,12]. Ceramides contribute to sphingolipid signaling and membrane stress, while phosphatidylethanolamine plasmalogens contribute to membrane organization and oxidative defense. Human brain studies report abnormalities in these and related lipid classes [13,14].

Biofluid studies have linked serum lipid profiles with later motor and non-motor outcomes [15] and identified metabolic differences in serum, plasma, and cerebrospinal fluid (CSF) [16–19]. Paired plasma and CSF measurements extend this approach across two compartments within the same participants. A shared clinical setting supports direct comparison of matrix-specific and integrated associations. This comparison is relevant to deciding which measurements deserve further longitudinal evaluation.

An interpretable panel provides a practical way to connect these biological questions with clinical trajectories. The panel comprised 16 provider-annotated anchors spanning BMP, ceramides, and plasmalogens, with fixed directional coding and transparent weighting.

Equal-analyte and class-balanced scores summarized the panel, alongside domain-specific and unsupervised comparators. This compact structure provides a manageable target for replication, assay assessment and focused biological follow-up.

Neural transcriptomes add another level of biological context for lipid-related questions. Midbrain and experimental studies implicate glial activation, mitochondrial metabolism, and astrocyte–neuron communication in PD [20–24]. Examining fatty-acid pathways in brain tissue and donor-level astrocyte data helps position a biofluid association within this broader setting. The transcriptomic comparisons therefore complement the longitudinal clinical question through their description of PD-related metabolic changes.

This exploratory secondary Parkinson's Progression Markers Initiative (PPMI) analysis examined whether integrated lipid scores were associated with the rate of PIGD change. Clinical adjustment, compartment comparisons, alternative longitudinal models, and influence analyses assessed the resulting association. The study links a fixed, biologically interpretable paired-biofluid panel with a domain-specific longitudinal outcome.

2. Materials and Methods

2.1. Study Design and Participants

This exploratory secondary analysis combined paired plasma and cerebrospinal fluid (CSF) lipid measurements with repeated clinical assessments from the Parkinson's Progression Markers Initiative (PPMI) [25]. Separately analyzed Gene Expression Omnibus datasets characterized lipid-related transcriptional changes in PD brain tissue and astrocytes.

The lipid panel was developed after exploratory metabolic analyses. Its composition, directional coding, and score definitions were fixed before the final lipid-specific longitudinal models; individual PIGD trajectories were not used to compute scores.

Among 213 participants with PD and paired plasma and CSF measurements at the same recorded clinical event, 193 met longitudinal eligibility and contributed 1152 assessments: 163 at index and 989 after index (Appendix A; Figure A1). Five participants lacked a complete eligible PIGD assessment, and 15 had no eligible post-index assessment. Eligibility required at least one observation more than 30 days after the index clinical-event month. The 213 paired participants formed the reference population for imputation and standardization. Median final follow-up was 5.17 years (IQR, 3.09–7.92; range, 0.25–13.00).

The molecular index was the earliest plasma lipidomics event with CSF measurements for the same participant and event identifier, ordered by age at visit. Events with unresolved timing ties were excluded. Plasma and CSF were thus matched at the clinical-event level; exact biospecimen collection intervals were unavailable.

PPMI is registered at ClinicalTrials.gov (NCT01141023). Its protocol was approved by the institutional review board or independent ethics committee at each participating center, and participants provided written informed consent [25]. De-identified PPMI data were analyzed under the applicable access and data-use requirements. The GEO analyses used publicly available de-identified data.

2.2. Cross-Compartment Lipid Integration Strategy

Plasma and CSF measurements were standardized within each matrix before averaging corresponding lipid features. Plasma-only, CSF-only, and integrated scores used the same anchors and longitudinal cohort, allowing direct comparison of their associations with PIGD change. Correlations between these scores described the relative contributions of the two compartments.

2.3. Metabolomic Preprocessing and Construction of Lipid Signatures

Targeted liquid chromatography–tandem mass spectrometry was performed on an Agilent Infinity II 1290 liquid chromatography system (Agilent Technologies, Santa Clara, CA, USA) coupled to a QTRAP 6500+ mass spectrometer (SCIEX, Framingham, MA, USA).The provider's protocol (Version 3, August 2024) covered both plasma and CSF and specified eight analytical batches per matrix, internal-standard normalization, pooled quality-control samples, and ComBat batch adjustment.

Preprocessing used positive, provider-adjusted area ratios. Lipids were matched by their original analyte identifiers, and duplicate participant–event–analyte records were excluded. Measurements were log2-transformed within each matrix. Features required at least 80% observed values in both matrices among the 213 paired participants; 110 shared features met this threshold. Remaining missing values were replaced by the matrix-specific feature median. Feature means and sample standard deviations were estimated in the same reference population. No further batch adjustment, winsorization, or outcome-based outlier exclusion was applied. The full feature annotation map is available from the corresponding authors on reasonable request.

For each retained analyte j, plasma and CSF measurements were independently standardized:

$$Z_{ij}^{P} = \frac{X_{ij}^{P} - \mu_{j}^{P}}{\sigma_{j}^{P}}, \tag{1}$$

and:

$$Z_{ij}^{C} = \frac{X_{ij}^{C} - \mu_{j}^{C}}{\sigma_{j}^{C}}, \tag{2}$$

For participant i and lipid j, P and C denote plasma and CSF, respectively. Means and sample standard deviations were calculated from log2-transformed, median-imputed measurements in the 213 paired participants.

The integrated value for each lipid was the mean of its standardized plasma and CSF measurements:

$$Z_{ij}^{paired} = \frac{Z_{ij}^{P} + Z_{ij}^{C}}{2}. \tag{3}$$

Each paired mean was standardized again across the 213 participants before directional coding and score construction. The resulting value summarizes a participant's relative lipid abundance across the two matrices.

The 16-lipid panel comprised provider-annotated BMP, ceramide, and phosphatidylethanolamine-plasmalogen features. Molecular names retain the assay's annotation level; no additional isomer, linkage, or positional characterization was performed.

The three BMP species were BMP(18:0_18:1), BMP(18:1/18:1) and BMP(22:6/22:6). The four ceramides were Cer(d18:1/16:0), Cer(d18:1/18:0), Cer(d18:1/24:0) and Cer(d18:1/24:1). The nine phosphatidylethanolamine plasmalogens were PE(P-16:0/20:4), PE(P-16:0/22:4), PE(P-16:0/22:6), PE(P-18:0/18:1), PE(P-18:0/18:2), PE(P-18:0/20:4), PE(P-18:0/22:6), PE(P-18:1/20:4) and PE(P-18:1/22:6).

In this notation, Cer(d18:1/16:0) identifies a ceramide annotated with a d18:1 long-chain base and a 16:0 acyl chain; PE(P-16:0/20:4) identifies a plasmalogen-annotated phosphatidylethanolamine.

The panel represented three aspects of lipid biology: endolysosomal lipid handling through BMP, sphingolipid metabolism through ceramides, and membrane organization and oxidative defense through plasmalogens [11–14]. Lipids were combined using fixed directions and equal weights, without fitting weights to PIGD outcomes.

BMP- and ceramide-labeled anchors received positive directions, while plasmalogen-labeled anchors received negative directions:

$$A_{ij} = d_j Z_{ij}^{paired}, \tag{4}$$

where $d_j = +1$ for BMP and ceramide species and $d_j = -1$ for plasmalogens.

The principal equal-analyte score was calculated as:

$$Score_i^{EA} = \frac{1}{16}\sum_{j=1}^{16} A_{ij}, \tag{5}$$

The score was subsequently standardized to zero mean and unit standard deviation.

A class-balanced score gave equal aggregate weight to the three domains. Domain means were first standardized:

$$B_i = Z\left(\frac{1}{3}\sum_{j\in BMP} A_{ij}\right), \tag{6}$$

$$C_i = Z\left(\frac{1}{4}\sum_{j\in CER} A_{ij}\right), \tag{7}$$

and:

$$P_i = Z\left(\frac{1}{9}\sum_{j\in PLS} A_{ij}\right). \tag{8}$$

The class-balanced score was then calculated as:

$$Score_i^{CB} = \frac{B_i + C_i + P_i}{3}, \tag{9}$$

followed by final standardization.

Comparator scores comprised the seven-anchor BMP–ceramide score, nine-anchor plasmalogen-deficit score, and first principal component (PC1) of all 110 shared features. PC1 explained 33.66% of variance and was oriented to align with the anchor-direction vector.

PC1 loading stability was assessed in 1000 participant-level bootstrap resamples. Resampled loading vectors were aligned to the original direction, and cosine similarity quantified agreement with the original loadings.

2.4. Definition of Longitudinal PIGD Progression

The primary longitudinal clinical outcome was the continuous postural instability and gait difficulty (PIGD) score derived from five items of the Movement Disorder Society-sponsored revision of the Unified Parkinson's Disease Rating Scale (MDS-UPDRS). These comprised NP2WALK and NP2FREZ from MDS-UPDRS Part II and NP3GAIT, NP3FRZGT and NP3PSTBL from Part III.

For participant i at clinical assessment t, PIGD was defined as:

$$PIGD_{it} = \frac{NP2WALK_{it} + NP2FREZ_{it} + NP3GAIT_{it} + NP3FRZGT_{it} + NP3PSTBL_{it}}{5} \tag{10}$$

All five items were required at each assessment. Values coded as 101 (unable to rate) were treated as missing. Outcomes were analyzed as observed, without longitudinal imputation.

The continuous PIGD composite ranges from 0 to 4 and captures change in the mean severity of gait, freezing, and postural impairment. Its distribution and floor effects were examined when assessing model suitability.

Part III examinations were selected using the recorded medication-state variables. Explicit OFF examinations took priority over untreated examinations; ON-only, unknown-state, and contradictory records were excluded. Identical duplicates were collapsed, and

conflicting equally eligible records were excluded. Part II and Part III assessments were matched by participant and clinical event, with component months separated by no more than 45 proxy days. A sensitivity model additionally included time-varying dopaminergic-treatment status.

Clinical dates were recorded to the month and represented by the first day of that month. The index date was the median of the Part II and Part III assessment months at the molecular event; each PIGD assessment was dated by the median of its component months. Index component spreads greater than 45 proxy days were excluded. Index assessments were retained in the repeated-outcome model. Follow-up intervals therefore refer to clinical-event timing rather than exact biospecimen collection dates. A stricter sensitivity analysis required components recorded in the same month and at least one observation more than 60 proxy days after index.

Follow-up time was expressed continuously in years:

$$Time_{it} = \frac{Date_{it} - Date_{index,i}}{365.25}. \tag{11}$$

The target estimate was the difference in annual PIGD change per 1-SD higher baseline lipid score, with the matched clinical-event month as the time origin.

2.5. Longitudinal Statistical Analysis

Associations between baseline lipid scores and longitudinal PIGD change were estimated using linear mixed-effects models. The reference model included fixed effects for follow-up time, baseline lipid score, the time-by-lipid-score interaction, centered age and sex, together with a participant-specific random intercept to account for within-participant correlation among repeated PIGD measurements:

$$\begin{aligned} PIGD_{it} \quad &= \beta_0 + \beta_1 Time_{it} + \beta_2 Score_i \\ &+ \beta_3 (Time_{it} \times Score_i) + \beta_4 Age_i + \beta_5 Sex_i \\ &+ u_i + \epsilon_{it}. \end{aligned} \tag{12}$$

The participant-specific intercept accounted for between-person variation in PIGD level. Alternative covariance structures and robust inference were examined in sensitivity analyses.

A clinically adjusted model added disease duration, index PIGD, index Part III severity excluding the three gait and postural items used in PIGD, dopaminergic-treatment status, and LRRK2 and GBA carrier indicators. These covariates, age and sex, also entered as interactions with time. Covariates were taken from the index event; eligible index motor data were available for 162 participants, contributing 1056 observations. Additional available-case models considered BMI and time-varying treatment. Lipid-modifying medication and other metabolic covariates were insufficiently documented for adjustment.

Mixed-effects models were fitted by restricted maximum likelihood using L-BFGS optimization. Results are expressed as annual differences in PIGD change per 1-SD higher lipid score, with 95% confidence intervals and two-sided p-values.

Five-year contrasts were calculated from the fitted annual interaction coefficients:

$$\Delta PIGD_{5y} = 5\beta_3. \tag{13}$$

These contrasts express the same fitted association over five years and were not analyzed as separate outcomes.

Benjamini–Hochberg correction was applied across the five lipid-score interaction tests [26]. Individual-anchor analyses formed a separate family of 16 tests. Nested models fitted by maximum likelihood on identical observations assessed the in-sample contribution of the score and its interaction with time beyond clinical covariates.

2.6. Sensitivity, Robustness and Influence Analyses

Sensitivity analyses examined the effects of covariance structure, clinical adjustment, follow-up definition and individual lipid contributions.

Generalized estimating equations (GEE) with an exchangeable working correlation and robust sandwich standard errors provided population-averaged estimates under an alternative treatment of within-participant correlation.

A mixed-effects model additionally allowed participant-specific slopes for follow-up time:

$$PIGD_{it} = X_{it}\beta + u_{0i} + u_{1i}Time_{it} + \epsilon_{it}. \quad (14)$$

Convergence and covariance estimates were examined, including variance-boundary warnings in the random-slope models.

Age-by-time and sex-by-time interactions allowed background PIGD trajectories to vary by these characteristics:

$$\begin{aligned} PIGD_{it} \quad &= \beta_0 + \beta_1 Time_{it} + \beta_2 Score_i + \beta_3 (Time_{it} \times Score_i) \\ &+ \beta_4 Age_i + \beta_5 Sex_i + \beta_6 (Time_{it} \times Age_i) \\ &+ \beta_7 (Time_{it} \times Sex_i) + u_i + \epsilon_{it}. \end{aligned} \quad (15)$$

Participant-level bootstrap inference used 1000 resamples with replacement for the reference and clinically adjusted models (seed, 20261111). All observations of a sampled participant were retained, and repeatedly sampled participants received separate cluster identifiers. Score definitions and standardization parameters were held fixed. Percentile 95% intervals quantified association uncertainty conditional on score construction. Further analyses used a common five-year follow-up window, post-index outcomes only, and quadratic time terms.

Leave-one-anchor analyses omitted each lipid in turn, reconstructed and standardized the score, and refitted the reference model using the same weighting rule.

Class-deletion analyses omitted BMP, ceramides, or plasmalogens to assess how each domain contributed to the composite association.

Follow-up sensitivities used an annual grid with ±0.5-year assessment windows. The latest recorded clinical month (September 2026) served as a proxy for observation opportunity. Stabilized inverse retention weights were estimated by logistic regression. Both weight models included quadratic nominal year, lipid score, age, and sex; the denominator model additionally included lagged PIGD, its missingness indicator, and prior visit count. Predicted probabilities were bounded at 0.02–0.98, and weights were truncated at the 1st and 99th percentiles. Weighted robust GEE included age-by-time and sex-by-time interactions. This analysis assessed sensitivity to measured differences in retention.

2.7. Independent Brain-Tissue and Single-Nucleus Transcriptomic Analyses

GSE168496, GSE136666 and GSE243639 were analyzed separately to characterize PD-related changes in lipid metabolism in brain tissue and astrocytes. These PD-versus-control comparisons provided a transcriptional context for the biofluid analysis.

GSE168496 comprised substantia nigra RNA sequencing from eight PD samples and eight controls [27]. Kallisto transcript-level estimated counts were mapped using Ensembl release 96, summed by gene, and rounded after aggregation. Genes with at least 10 counts in three samples were retained (17,994 genes). The reference model was ~ sex + condition; separate sensitivity models added standardized age or post-mortem interval (PMI). These covariates were complete for all 16 samples.

GSE136666 contained five PD and five control substantia nigra pools, with two donors per pool, and three PD and three control putamen pools, with three donors per pool [28].

Each pool was one experimental unit. Kallisto estimated counts were mapped using Ensembl release 86, summed by gene, and rounded. Genes with at least 10 counts in three substantia nigra pools or two putamen pools were retained (22,280 and 22,402 genes). Regional comparisons used ~ condition, with sex-adjusted models and exclusion of QC-flagged pools GSM4054769 and GSM4054776 as sensitivities. Constituent donor identifiers were unavailable, so overlap between regions or with GSE168496, also derived from the Netherlands Brain Bank, could not be assessed.

GSE243639 comprised 83,484 filtered nuclei from 15 PD donors and 14 controls [29]. Donor pseudobulk profiles summed integer counts within the broad Astro annotation, comprising 20,710 nuclei. Each donor contributed 174–1830 astrocytic nuclei (median, 711); no additional nucleus-count threshold was imposed. Descriptive six-subcluster UMAP coordinates were available for 16,322 of these nuclei. Genes with at least 10 counts in five donors were retained (16,785 genes).

Available UMAP coordinates and cell labels were used to describe the annotated astrocyte subset; differential-expression inference was conducted at the donor level.

The primary astrocyte model was ~ age_z + sex + pmi_z + rin_z + condition, with standardized continuous covariates. Age, sex, PMI, and RNA integrity number were complete. The source study combined reads from both sequencing runs for 13 resequenced libraries. A sensitivity model added a binary resequencing indicator, and a QC sensitivity excluded Astro__D002, leaving 14 PD donors and 14 controls. These specifications reused the same donor cohort. Counts were normalized using PyDESeq2 size factors and negative binomial models without prior log transformation. Bulk results were not corrected for estimated cell fractions. Exploratory donor-level composition models used centered log-ratio abundances, age, sex, PMI, and RNA integrity covariates, HC3 standard errors, and BH correction within annotation family. These models cannot eliminate composition-related confounding.

2.8. Differential-Expression, Pathway-Enrichment and Cross-Dataset Convergence Analyses

Differential-expression analyses treated individual samples as the experimental unit in GSE168496, tissue pools in GSE136666, and donor-level cell-type pseudobulk profiles in GSE243639. Table A1 summarizes the experimental units and primary models. Appendix B provides additional details on filtering, covariates, and enrichment settings.

Count-based differential expression used PyDESeq2, an implementation of the DESeq2 framework [30]. Gene-level adjusted *p*-values used the Benjamini–Hochberg procedure. Count aggregation and filtering followed the dataset-specific procedures described in Section 2.7 and Appendix B.

Preranked gene-set enrichment analysis [31] ordered genes by the signed PD-versus-control Wald statistic. Gene symbols were uppercased; duplicates were represented by the entry with the highest mean normalized abundance and deterministic identifier tie-breaking. Entries lacking finite ranking statistics or raw *p*-values were excluded. GSEApy used weight 1, 10,000 gene-set permutations, and 15–500 overlapping genes per set. Seeds were 168496, 136666, and 243639, respectively. The Enrichr collections MSigDB_Hallmark_2020, KEGG_2021_Human and Reactome_2022 were used across datasets.

Eight lipid-related pathways were selected for display from the exploratory survey: Hallmark Fatty Acid Metabolism, KEGG Fatty Acid Degradation, Reactome Mitochondrial Fatty Acid Beta-Oxidation, Hallmark Bile Acid Metabolism, Reactome Peroxisomal Lipid Metabolism, KEGG Biosynthesis of Unsaturated Fatty Acids, Reactome Fatty Acid Metabolism and KEGG Fatty Acid Elongation. Multiplicity correction used the full eligible source libraries, as described below.

Negative normalized enrichment scores (NESs) indicate lower pathway-level transcription in PD. GSEApy permutation-based FDR q-values were computed within each full eligible library and model before pathways were selected for display. Table A2 reports the number of eligible pathways in each testing family. Table A3 reports all eight displayed pathways across the ten analysis contexts. Complete full-library results and exact gene-set definitions are available from the corresponding authors on reasonable request.

Pathways were compared across GSE168496 substantia nigra, GSE136666 substantia nigra and putamen, and three model specifications in the GSE243639 astrocyte cohort. Regions and repeated specifications were interpreted within their source cohorts.

Tissue and subpopulation composition were considered when interpreting pathway differences. These analyses characterized PD-related pathway differences in tissue and cell-type contexts.

2.9. Statistical Reporting and Software

Clinical effects are reported with 95% confidence intervals. Gene-level and pathway-level multiplicity corrections were applied within the testing families described above. All statistical tests were two-sided.

Clinical analyses used Python 3.12.3 and statsmodels 0.14.6. Transcriptomic differential-expression models used PyDESeq2 0.5.4, and preranked enrichment used GSEApy 1.3.1. Additional analytical settings are reported in Appendices A–C.

3. Results

3.1. Cohort and Lipid Score Characteristics

The longitudinal cohort included 193 participants (107 men and 86 women), with a mean index age of 64.10 years (SD, 7.99). Median disease duration was 2.25 years (IQR, 1.25–4.25); index motor measures and assessment state were available for 162 participants. Their median PIGD was 0.30 (IQR, 0.20–0.40), non-gait Part III score 23.0 (15.25–30.0), and Hoehn and Yahr stage 2.0 (1.0–2.0). Of these participants, 106 were examined OFF medication, and 56 were untreated. Among all 193 participants, 70 carried LRRK2 variants, and 22 carried GBA variants. Median BMI was 26.39 kg/m^2 (IQR, 23.68–30.00; $n = 180$). Table 1 gives the available denominator for each clinical characteristic.

The 213 participants with paired plasma and CSF measurements formed the score reference population. All 110 shared lipid features met the 80% observation threshold. The 16-anchor panel comprised three BMP, four ceramide, and nine plasmalogen annotations (Figure 1A). Both matrices had complete observations for 15 of the 16 panel anchors. BMP(22:6/22:6) was observed in 195/213 plasma and 212/213 CSF samples, and missing values were imputed before standardization.

The equal-analyte score assigned equal weight to all 16 directionally coded anchors. The class-balanced score assigned equal aggregate weight to the standardized BMP, ceramide, and plasmalogen blocks. Comparator scores summarized the BMP–ceramide anchors, plasmalogen anchors, and first principal component (PC1) of all 110 shared features.



Figure 1. Exploratory lipid-score construction and reference-model associations. (**A**) Observation coverage of the 16 source-labeled anchors in plasma and CSF. The panel contains three BMP, four ceramide, and nine plasmalogen features; signs indicate score coding. (**B**) Age- and sex-adjusted score-by-time estimates with model-based 95% confidence intervals. BH q-values refer to the five tests. (**C**) PCA of eight PD and eight control GSE168496 substantia nigra samples. (**D**) Sex-adjusted differential expression in the same dataset. Axes show log2 fold change and −log10 adjusted *p*-value. Two transcripts are annotated; dashed lines mark adjusted $p = 0.05$ and log2 fold changes of ±1. Panels (**C**,**D**) provide separate transcriptomic context. BMP, bis(monoacylglycerol) phosphate; CSF, cerebrospinal fluid; PIGD, postural instability and gait difficulty; BH, Benjamini–Hochberg.

Table 1. Characteristics of the longitudinal clinical analysis.

Participant Characteristic	Value and Available Denominator
Longitudinal cohort	193 participants with PD
Age at index, years	64.10 (SD 7.99); $n = 193$
Men/women	107/86; $n = 193$
Disease duration, years	2.25 (IQR 1.25–4.25); $n = 193$
Index PIGD, 0–4	0.30 (IQR 0.20–0.40); $n = 162$; missing 31
Index total MDS-UPDRS Part III	24.0 (IQR 16.0–31.0); $n = 162$; missing 31
Index non-gait Part III	23.0 (IQR 15.25–30.0); $n = 162$; missing 31
Index Hoehn and Yahr stage	2.0 (IQR 1.0–2.0); $n = 162$; missing 31
Eligible index examination state	106 treated OFF; 56 untreated; missing 31
LRRK2 carrier/GBA carrier	70/22; $n = 193$ for each indicator
BMI, kg/m^2	26.39 (IQR 23.68–30.00); $n = 180$; missing 13
Last eligible follow-up, years	5.17 (IQR 3.09–7.92); range 0.25–13.00; $n = 193$
Observations per participant	6 (IQR 3–8); range 1–15
Clinical observations	1152 total; 163 at time zero; 989 after time zero
All-observation PIGD, mean (SD)	0.541 (0.523); $n = 1152$ observations
All-observation PIGD range	0–3.8; 144/1152 (12.5%) at zero

PC1 explained 33.66% of variation across the 110 shared lipid features. The loading-vector cosine similarity interval was 0.992–0.998 across the original 1000 participant bootstrap resamples, indicating stable loadings within this reference population.

3.2. Exploratory Associations with Longitudinal PIGD Change

The reference mixed models yielded positive time interactions for the equal-analyte and class-balanced scores (Figure 1B; Table 2). Each 1-SD higher equal-analyte score corresponded to an additional annual PIGD increase of 0.01248 units (model-based 95% CI, 0.00447–0.02048; $p = 0.00225$; q = 0.00563). The class-balanced estimate was 0.01438 units/year per SD (model-based 95% CI, 0.00599–0.02278; $p = 0.000785$; q = 0.00392). Both q-values refer to the exploratory five-score testing family.

Table 2. Reference-model associations between the five lipid scores and longitudinal PIGD change.

Lipid Signature	Annual β per 1-SD	95% CI	*p*-Value	BH q-Value
Equal-analyte integrated score	0.01248	0.00447 to 0.02048	0.00225	0.00563
Class-balanced integrated score	0.01438	0.00599 to 0.02278	0.000785	0.00392
BMP–ceramide burden	0.00618	−0.00166 to 0.01401	0.122	0.204
Plasmalogen-deficit score	0.00525	−0.00235 to 0.01285	0.176	0.22
Lipid PC1	−0.00116	−0.00857 to 0.00625	0.758	0.758

The BMP–ceramide and plasmalogen-deficit estimates were smaller, with model-based intervals spanning zero. PC1 showed little association with longitudinal PIGD change in the reference model (Table 2).

Figure 1C,D shows the principal-component and differential-expression profiles of GSE168496, providing a transcriptomic view of PD-related molecular variation.

3.3. Fatty-Acid Metabolic Programs Show Convergent Downregulation Across PD Brain Regions

Independent PD-versus-control transcriptomic comparisons examined fatty-acid metabolic pathways. Because these datasets do not measure the clinical lipid panel, enrichment direction cannot be directly linked to its score orientation.

In the primary GSE168496 substantia nigra analysis, Hallmark Fatty Acid Metabolism showed marked negative enrichment in PD (NES = −2.286, FDR < 0.0001). Related pathways showed the same direction, including KEGG Fatty Acid Degradation (NES = −2.263,

FDR = 0.000020), Reactome Mitochondrial Fatty Acid Beta-Oxidation (NES = −2.166, FDR = 0.000084), Reactome Peroxisomal Lipid Metabolism (NES = −2.009, FDR = 0.000915) and KEGG Fatty Acid Elongation (NES = −1.749, FDR = 0.0102).

The direction of these pathway alterations was reproduced in the separately deposited GSE136666 regional dataset. Hallmark Fatty Acid Metabolism was negatively enriched in both pooled substantia nigra samples (NES = −1.761, FDR = 0.00468) and pooled putamen samples (NES = −1.768, FDR = 0.00687). Mitochondrial fatty-acid β-oxidation was similarly reduced in substantia nigra (NES = −1.943, FDR = 0.00261) and putamen (NES = −1.692, FDR = 0.0410), while Fatty Acid Elongation showed negative enrichment in substantia nigra (NES = −1.537, FDR = 0.0445) and putamen (NES = −1.983, FDR = 0.00173).

Excluding the QC-flagged substantia nigra pool changed the number of condition-only gene-level findings at FDR < 0.05 from 178 to 473, with 158 shared findings. Among 95 metabolic-domain pathway rows, 90 retained the same NES direction, and 39 met the FDR threshold in both analyses. Table A3 presents the lipid-pathway sensitivity results; complete exclusion results are available from the corresponding authors upon reasonable request.

Negative enrichment recurred across the displayed pathways, with variable FDR support between regions (Figure 2A,B). These comparisons describe transcriptomic patterns in PD tissue rather than longitudinal clinical validation.

3.4. Donor-Level Astrocyte Pathway Analyses

GSE243639 contained 83,484 annotated nuclei from 29 donors, including 15 PD and 14 controls. The broad Astro annotation included the 20,710 nuclei used for donor-level pseudobulk analysis. Descriptive six-subcluster UMAP coordinates covered 16,322 of these nuclei (78.8%; Figure 2C,D).

Astrocyte counts ranged from 174 to 1830 per donor, with a median of 711. The donor-level PCA and differential-expression plots summarize these pseudobulk profiles (Figure 2E,F). Nuclei were not treated as independent biological replicates.

At the pathway level, Hallmark Fatty Acid Metabolism showed the most reproducible negative enrichment across the three astrocyte analytical specifications. The pathway was negatively enriched in the primary analysis (NES = −2.189, FDR < 0.0001), in the resequencing-adjusted analysis (NES = −2.180, FDR < 0.0001), and after the QC-exclusion sensitivity (NES = −2.267, FDR = 0.000081).

KEGG Fatty Acid Degradation showed similarly reproducible negative enrichment in the primary analysis (NES = −1.947, FDR = 0.00305), resequencing-adjusted analysis (NES = −1.807, FDR = 0.0107), and QC-exclusion analysis (NES = −1.926, FDR = 0.00382).

Other lipid-related pathways showed directionally similar but less uniform statistical support. Mitochondrial Fatty Acid Beta-Oxidation was negatively enriched in the primary astrocyte analysis (NES = −1.739, FDR = 0.0250) and QC-exclusion analysis (NES = −1.738, FDR = 0.0211), whereas the resequencing-adjusted specification was less precise (NES = −1.486, FDR = 0.114). Fatty Acid Elongation showed a similar pattern, with negative enrichment in the primary analysis (NES = −1.601, FDR = 0.0452) and QC-exclusion analysis (NES = −1.576, FDR = 0.0431), but not in the resequencing-adjusted specification.

Hallmark Fatty Acid Metabolism met the pathway FDR threshold in all six displayed tissue and model contexts (Figure 2A,B). These contexts included regional analyses and repeated specifications within the same donor cohorts.

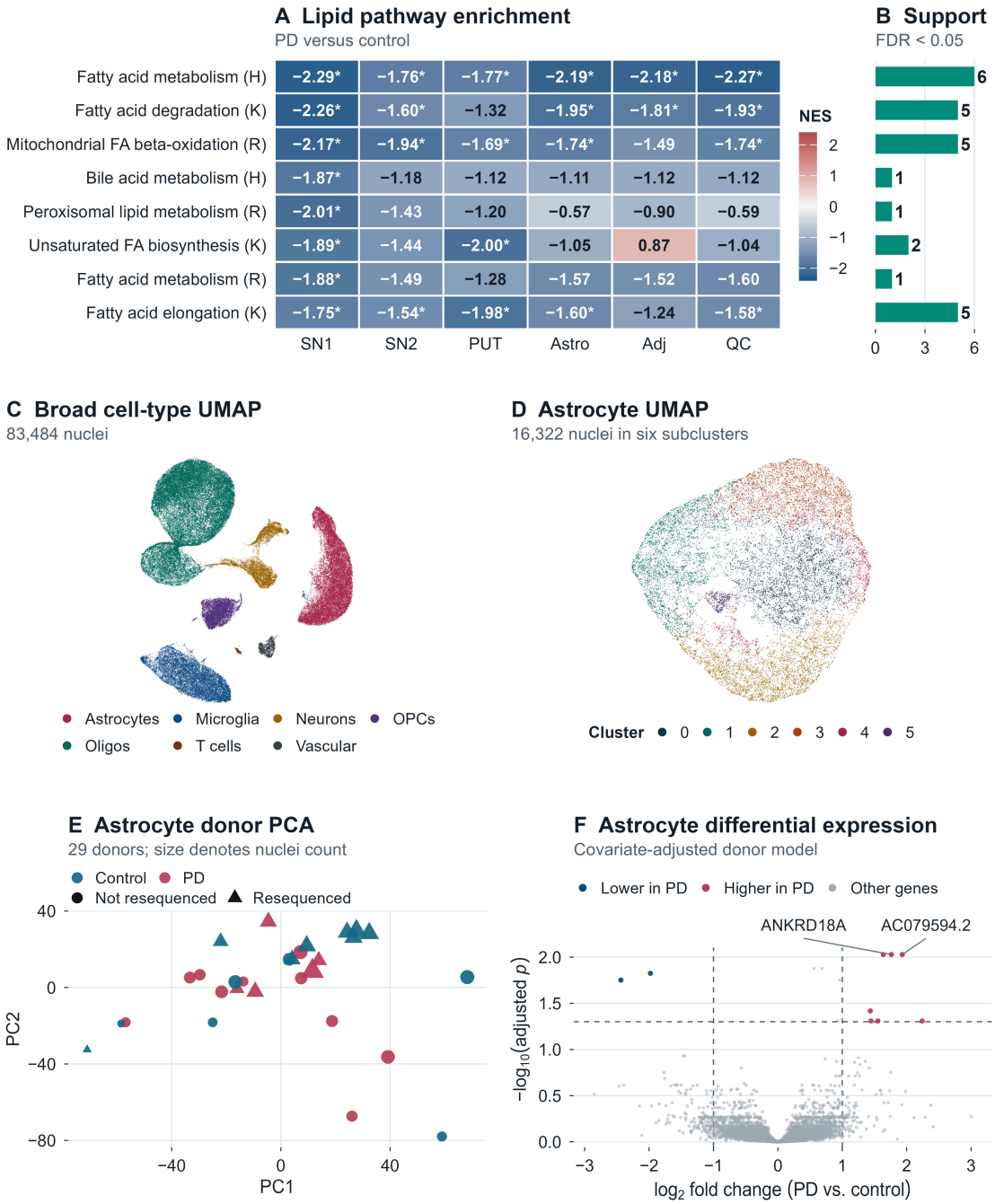


Figure 2. Lipid pathway enrichment and donor-level astrocyte analyses in PD. (**A**) Normalized enrichment scores (NES) for eight lipid-related pathways. SN1, GSE168496 substantia nigra; SN2 and PUT, GSE136666 substantia nigra and putamen. Astro, Adj, and QC denote the GSE243639 primary, resequencing-adjusted, and donor-QC-exclusion astrocyte models. Negative NES indicates enrichment toward the control end of the PD-versus-control ranking. Asterisks mark FDR < 0.05 within each library and model. H, K, and R denote Hallmark, KEGG, and Reactome. (**B**) Contexts meeting FDR < 0.05 per pathway (of six; not independent replications). (**C**) Broad cell-type UMAP of 83,484 GSE243639 nuclei. (**D**) Descriptive UMAP of 16,322 nuclei in six astrocyte subclusters, a subset of the 20,710 nuclei used for pseudobulk analysis. (**E**) PCA of 29 donor pseudobulk profiles (15 PD, 14 controls). Color, shape, and size denote diagnosis, resequencing status, and nuclei count per donor, respectively. (**F**) Donor-level differential expression for PD versus control, adjusted for age, sex, post-mortem interval, and RNA integrity number. Dashed lines mark Benjamini–Hochberg-adjusted $p = 0.05$ and $\log_2$ fold change $= \pm 1$. Colored points meet adjusted $p < 0.05$ and $|\log_2 \text{ fold change}| \geq 1$; gray denotes all other genes. Labels were selected by adjusted p-value, breaking ties by larger absolute $\log_2$ fold change.

None of the 31 donor-level composition components tested across the annotation families passed the corresponding within-family BH threshold. The sample size and incomplete subcluster annotation nevertheless limit the ability to exclude composition effects.

The donor-level astrocyte analysis identified lower expression of fatty-acid metabolic pathways in PD, complementing the broader brain-tissue observations.

3.5. Effect Magnitude and Longitudinal Model Comparisons

Figure 3A shows fixed-effect mean PIGD trajectories over five years at −1, 0, and +1 SD of the equal-analyte score. Time zero corresponds to the matched clinical-event month used as the index proxy.

The equal-analyte five-year contrast was 0.0624 PIGD units per SD (model-based 95% CI, 0.0224–0.1024), compared with 0.0719 for the class-balanced score (Figure 3C). The reference model's time coefficient was 0.06967 units/year, equivalent to 0.3483 units over five years at its reference values. The equal-analyte contrast was approximately 18% of that fitted change, with a small absolute magnitude on the 0–4 scale. Clinical importance for this five-item mean was not established in this study.

Robust GEE gave an equal-analyte estimate similar to the reference mixed model, with a wider interval that included zero (Figure 3B). The estimate was 0.01231 units/year per SD (95% CI, −0.00189–0.02651; $p = 0.0893$).

The random-slope estimate was 0.01893 units/year per SD (95% CI, 0.00094–0.03692; $p = 0.0391$). A variance-boundary warning limited reliance on its nominal confidence interval.

Allowing background trajectories to vary with age and sex yielded a random-intercept estimate of 0.01314 (95% CI, 0.00504–0.02123; $p = 0.00147$). Corresponding GEE and random-slope estimates were 0.01291 (95% CI, 0.00017–0.02565) and 0.01972 (0.00225–0.03718), respectively. The random-slope model again produced a variance-boundary warning; covariance diagnostics are summarized in Appendix C.

Participant-level bootstrap inference gave wider equal-analyte percentile 95% intervals: −0.00575–0.02503 for the reference model and −0.00241–0.02950 after clinical adjustment. Each analysis used 1000 valid resamples, and both intervals included zero. Statistical support therefore depended on the inference method, despite broadly similar point estimates. Tables A4 and A5 report the complete fixed-effect coefficients for the reference and clinically adjusted equal-analyte mixed models, respectively. Table A6 reports the clinically adjusted mixed-model and GEE results for all five scores.

Figure 3D,E presents PCA and expression profiles for GSE136666 substantia nigra tissue pools, extending the transcriptomic comparison to a second deposited brain dataset. Each pooled tissue sample served as the experimental unit for these analyses.

3.6. Anchor Influence and Structural Stability

All 16 leave-one-anchor estimates were positive, ranging from 0.01013 to 0.01424 PIGD units/year per SD, compared with 0.01248 for the full panel (Figure 4A). Omitting BMP(18:0_18:1) gave the smallest estimate, whereas omitting PE(P-18:0/18:1) gave the largest. Table A7 reports the individual-anchor associations, and Table A8 reports all anchor-omission estimates and confidence intervals.

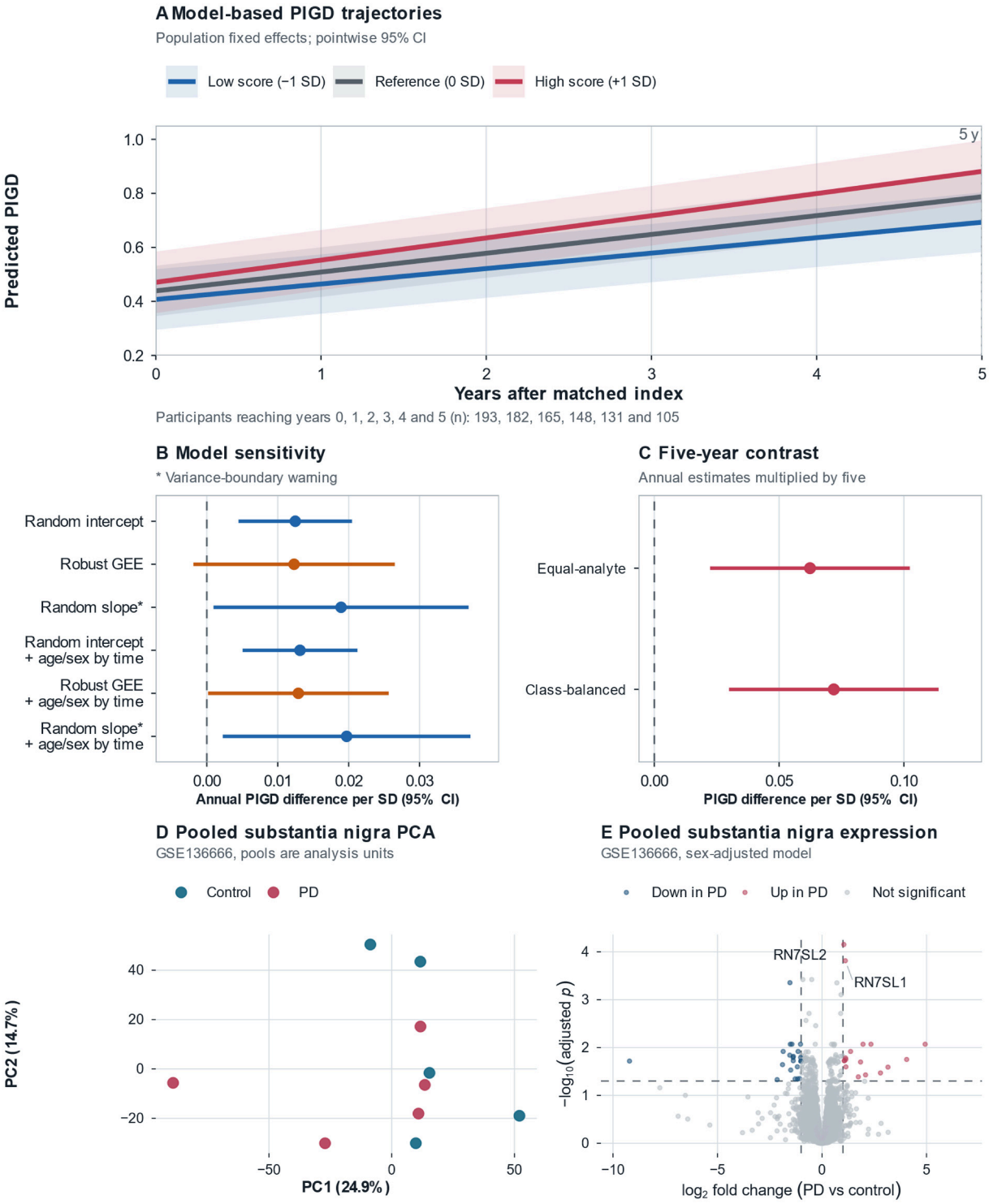


Figure 3. PIGD trajectories and longitudinal model comparisons. (**A**) Fixed-effect mean trajectories at −1, 0, and +1 SD of the equal-analyte score, at mean-centered age and reference sex. Shading denotes pointwise 95% confidence intervals. Counts indicate participants whose final follow-up reached each year. The time axis uses the matched clinical-event month. (**B**) Score-by-time estimates and 95% intervals from random-intercept, robust GEE, and random-slope models, with age-by-time and sex-by-time terms where indicated. Asterisks denote variance-boundary warnings. (**C**) Five-year contrasts calculated as five times the annual interaction coefficient and confidence limits. (**D**) PCA of pooled GSE136666 substantia nigra samples. (**E**) Sex-adjusted differential expression for the same pools. Dashed lines denote adjusted $p = 0.05$ and log2 fold change = ±1. Two transcripts are annotated by increasing finite adjusted p-value. Tissue pools are the experimental units in panels (**D**,**E**).

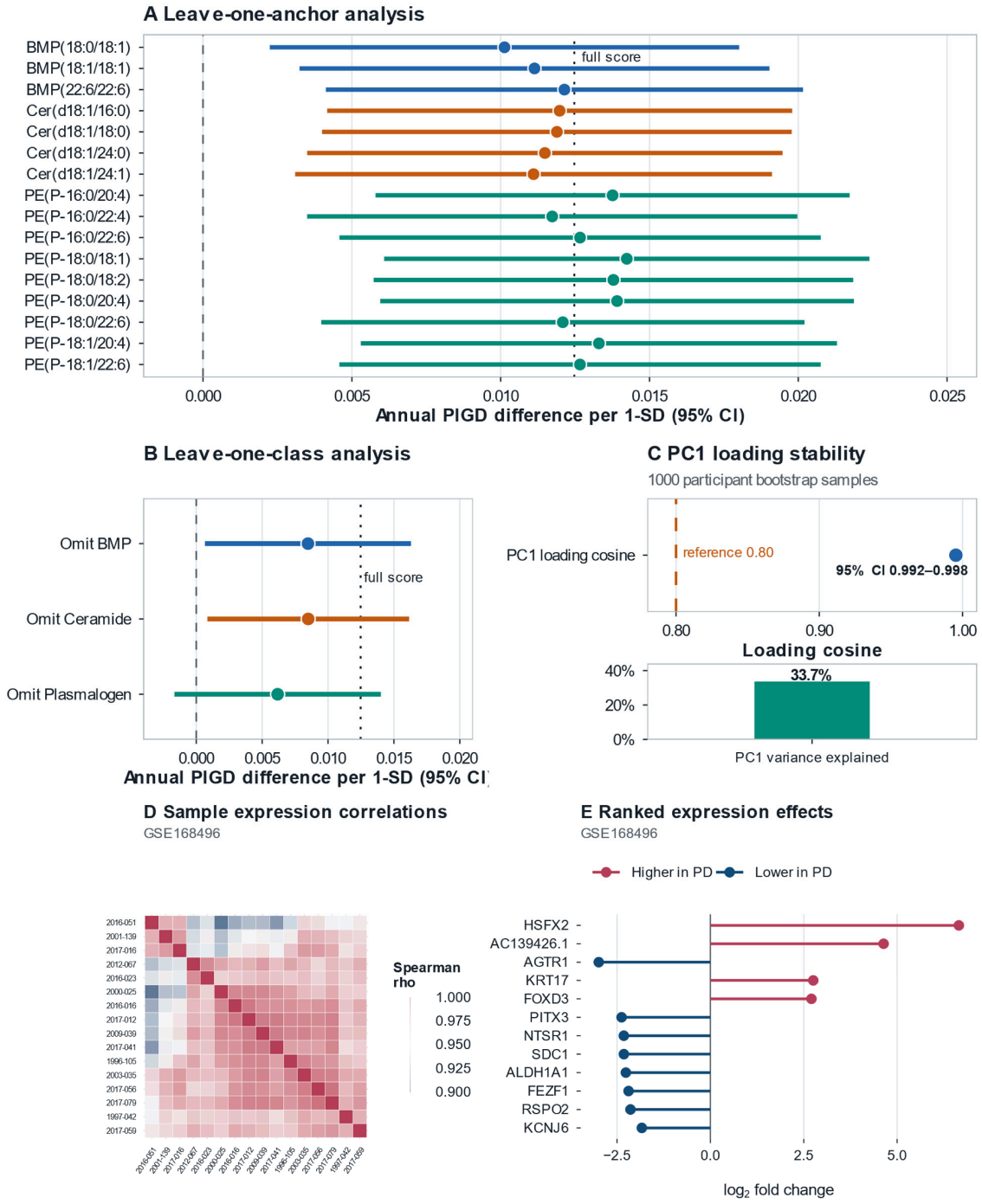


Figure 4. Exploratory anchor influence and molecular-axis stability. (**A**) Annual score-by-time coefficients after omitting each of the 16 source-labeled anchors in turn. Points and horizontal lines show estimates and 95% confidence intervals from the reconstructed equal-analyte reference model. The dotted vertical line marks the full-panel estimate. (**B**) Corresponding leave-one-class analyses after omission of BMP, ceramides, or plasmalogens. (**C**) PC1 loading-vector cosine similarity from 1000 participant-level bootstrap samples. The displayed empirical 95% interval is 0.992–0.998; the dashed line marks a descriptive reference of 0.80. The lower panel shows that PC1 explained 33.7% of the lipid-matrix variance. Loading agreement quantifies structural stability. (**D**) Hierarchically ordered sample Spearman correlations for GSE168496 substantia nigra. (**E**) Twelve selected GSE168496 transcripts ranked by absolute log2 fold change among genes with adjusted $p < 0.05$ and absolute log2 fold change ≥1. Positive values indicate higher expression in PD and negative values indicate lower expression. Panels (**D**,**E**) provide descriptive transcriptomic quality context. BMP, bis(monoacylglycerol) phosphate; PC1, principal component 1; PIGD, postural instability and gait difficulty.

Class-deletion estimates were 0.00848 after omitting BMP, 0.00850 after omitting ceramides, and 0.00618 after omitting plasmalogens (Figure 4B). The estimates describe sensitivity of the composite association to removal of each lipid domain.

The stable PC1 loading structure (Figure 4C) coexisted with little evidence of a PIGD association in the reference model (Table 2). Table A9 reports the oriented loadings for all 110 shared lipid features.

Sample correlations and ranked expression effects in GSE168496 summarize cohort structure and the distribution of PD–control differences (Figure 4D,E).

3.7. Clinical Adjustment and Compartment-Specific Associations

Clinical adjustment yielded an equal-analyte estimate of 0.01408 PIGD units/year per SD (model-based 95% CI, 0.00646–0.02170; 162 participants, 1056 observations). Robust GEE gave 0.01402 (95% CI, 0.00168–0.02636). Bootstrap intervals for both mixed models are reported in Section 3.5 and Table 3; covariance and convergence diagnostics are summarized in Appendix C.

Table 3. Equal-analyte effects and uncertainty under clinical adjustment and alternative inference. Annual effects are PIGD units/year per SD. Bootstrap intervals use 1000 participant resamples per model and fixed score-construction parameters.

Specification	Participants/ Observations	Annual Estimate	95% Interval
Reference random intercept	193/1152	0.01248	0.00447 to 0.02048
Reference robust GEE	193/1152	0.01231	−0.00189 to 0.02651
Reference participant bootstrap	193/1152	0.01248	−0.00575 to 0.02503
Clinically adjusted random intercept	162/1056	0.01408	0.00646 to 0.02170
Clinically adjusted robust GEE	162/1056	0.01402	0.00168 to 0.02636
Clinically adjusted participant bootstrap	162/1056	0.01408	−0.00241 to 0.02950
Plasma-only equal-analyte	193/1152	0.01144	0.00278 to 0.02011
CSF-only equal-analyte	193/1152	0.00766	0.00036 to 0.01495

In the same 193 participants, plasma-only and CSF-only equal-analyte estimates were 0.01144 (95% CI, 0.00278–0.02011) and 0.00766 (0.00036–0.01495), respectively. Adding the score and its time interaction to the clinical model improved in-sample fit (likelihood ratio, 18.58; 2 df; $p = 0.0000923$). AIC decreased from 713.69 to 699.11; prediction error and calibration in new participants were not evaluated.

Plasma-only and CSF-only scores correlated at r = 0.165 in the longitudinal sample. Their correlations with the integrated score were 0.885 and 0.604, respectively. Among the 16 individual-anchor tests, two met the separate BH threshold, including a plasmalogen feature with a negative unaligned association. Table A7 reports all individual-anchor results; the full score correlation matrix is available from the corresponding authors on reasonable request.

Participants contributed a median of six observations (IQR, 3–8); nine had one observation, and 21 had one post-index observation. Follow-up reached 3, 5, 7 and 10 years for 148, 105, 60 and 13 participants, respectively. PIGD was zero in 144/1152 observations (12.5%), with no ceiling values. Distributional, covariance, and residual diagnostics are reported in Appendix C.

Restricting follow-up to five years yielded 0.02056 (95% CI, 0.00691–0.03420; 187 participants), while stricter same-month component matching yielded 0.01257 (0.00456–0.02059; 193 participants). Participants with shorter follow-up were older and had higher available index PIGD. Inverse-retention-weighted GEE yielded 0.01796 (0.00381–0.03212), con-

ditional on the modeled observation opportunity and measured predictors of retention (Appendix C).

Restricting the baseline-conditioned clinical model to post-index outcomes gave 0.01305 (model-based 95% CI, 0.00399–0.02210; 162 participants, 893 observations). Robust GEE yielded 0.01287 (95% CI, −0.00055–0.02628), and the 1000-resample participant-bootstrap interval was −0.00521–0.02839. No score met the five-score BH threshold in the clinically adjusted GEE analysis (equal-analyte q = 0.0648; class-balanced q = 0.0514). Table A6 reports the complete five-score clinical sensitivity family.

4. Discussion

This study extends the investigation of PD lipid abnormalities to a defined longitudinal motor domain. Higher integrated plasma and CSF scores were associated with steeper PIGD change in the reference mixed models. The estimate remained similar after adjustment for disease duration, index severity, genotype, and treatment. Paired measurements permitted direct matrix-specific comparisons within the same participants. The fixed 16-lipid panel and transparent weighting provide a clearly specified basis for independent testing of the relationship between lipid variation and axial progression.

The reference five-year contrast of 0.0624 PIGD units was approximately 18% of the fitted time-related change at the model's reference values. Its absolute magnitude was small on the 0–4 scale, and its clinical importance was not established in this study. The composite reflects clinical ratings of gait, freezing and postural impairment. Relating the panel to instrumented gait, falls, and daily function would determine whether the group-level association captures changes that matter to patients. Such comparisons would give subsequent stratification studies an explicit clinical target.

BMP, ceramides and plasmalogens represent complementary aspects of membrane biology. BMP participates in endolysosomal lipid handling, ceramides in sphingolipid signaling and membrane stress, and plasmalogens in membrane organization and oxidative defense [11–14]. These roles suggest plausible connections with neuronal membranes, organelles, and metabolic support. Directional coding expresses a combined hypothesis across these processes in an interpretable score. The reference association persisted across individual anchor omissions, while class deletions changed its magnitude. These results motivate focused examination of the domains and their covariance, including whether the same combination accompanies axial deterioration in another longitudinal cohort.

Matrix-specific comparisons help define the measurement strategy that warrants further evaluation. Plasma-only and CSF-only estimates were positive in the same participants, allowing the observed pattern to be examined within each compartment. Plasma and CSF scores were modestly correlated, and the integrated score tracked plasma-only variation more closely than CSF-only variation. A prospective comparison can determine whether CSF adds information beyond plasma and clinical measures. Plasma offers a less-invasive route for studying the fixed panel. The practical objective is to identify a reproducible assay configuration whose additional information justifies the sampling requirements.

The brain and astrocyte findings place the clinical analysis alongside broader PD-related metabolic alterations [13,14,20–24]. Reduced fatty-acid pathway expression across the examined contexts describes lipid-related biology at the transcriptional level. Regional brain and donor-level astrocyte analyses contribute tissue and cell-type perspectives to this setting. Their value lies in refining the biological questions for subsequent work. Participant-matched molecular studies could test whether the biofluid pattern relates to specific cellular metabolic states and help explain the longitudinal clinical association.

Biological stratification is a potential research application of this panel. Its fixed 16-anchor format provides a manageable target for assay validation and cross-cohort replication.

Prospective studies could evaluate the continuous score for identifying groups with reproducibly different molecular profiles and axial trajectories. Clinical-trial enrichment would become a relevant application if the score adds useful progression information beyond established clinical variables. Evaluation should address a defined research decision, including the size of the trajectory difference, stability across cohorts, and contribution of each biofluid.

The exploratory post hoc design is the principal limitation; five-score correction does not encompass the preceding selection history. Participant-bootstrap intervals included zero, and reference GEE provided weaker statistical support than the model-based mixed-model intervals. Residual non-normality and heteroscedasticity also make the evidence sensitive to inference methods. Month-level clinical timing and unavailable exact collection intervals limit temporal precision, while provider annotations constrain molecular structural specificity. Incomplete clinical covariates, medication histories, complete-item selection, and differential follow-up introduce potential confounding and selection effects. The separate neural datasets provide pathway context; tissue composition, pooling, and possible donor overlap constrain mechanistic and replication interpretation. External prediction, calibration, and patient-level clinical utility remain to be evaluated.

Independent longitudinal evaluation should fix the panel, directional coding, and preprocessing before outcome analysis. Precisely documented paired sampling and standardized clinical assessments would improve the interpretation of temporal relationships. Clinical and clinical-plus-lipid models should be compared using participant-level prediction error and calibration in new data. A planned plasma-only comparison would assess the information gained from CSF and the feasibility of a less-invasive configuration. Instrumented gait, falls, and functional outcomes would provide an external clinical reference for the PIGD contrast. These evaluations would establish whether the association can support a useful research stratification strategy.

5. Conclusions

This study connects a fixed 16-lipid panel from paired plasma and CSF measurements with longitudinal axial motor progression in PD. Reference models linked higher integrated scores to steeper PIGD change, with a small absolute effect and inference-dependent statistical support. The biologically interpretable panel provides a focused target for independent replication and assay evaluation. Prospective studies could determine whether it supports biological stratification, clinical-trial enrichment, or a practical plasma-based assessment strategy, with value defined by improvements beyond established clinical measures.

Author Contributions: Y.Q. and Y.C. contributed equally to this work. Conceptualization, Y.Q., Y.C., M.W. and T.W.; methodology, Y.C. and H.G.; formal analysis, Y.C. and H.G.; investigation, Y.Q., Y.C. and H.G.; data curation, Y.C., H.G., X.L., X.W., W.Z., Z.W. (Zhuoya Wang) and Z.W. (Zimu Wu); validation, Y.C. and H.G.; visualization, Y.C. and H.G.; writing—original draft preparation, Y.Q. and Y.C.; writing—review and editing, all authors; supervision, M.W. and T.W.; project administration, M.W. and T.W.; funding acquisition, M.W. and T.W. All authors have read and agreed to the published version of the manuscript.

Funding: This research was funded by the Natural Science Foundation of Shandong Province (grant number ZR2026QC0920), the Science and Technology Development Fund of Tianjin Education Commission for Higher Education (grant number 2022KJ143), and the National College Students' Innovation and Entrepreneurship Training Program (grant number 202610063002). The funders had no role in study design, data collection, analysis, interpretation, or manuscript preparation.

Institutional Review Board Statement: The study was conducted in accordance with the Declaration of Helsinki and applicable ethical requirements. The original PPMI protocol was approved by the institutional review board or independent ethics committee at each participating site be-

fore study initiation. PPMI is registered at ClinicalTrials.gov under identifier NCT01141023. The present study involved secondary analysis of de-identified PPMI data and publicly available transcriptomic datasets, without additional participant recruitment, intervention, or biospecimen collection. GSE168496 and GSE136666 used post-mortem tissue from the Netherlands Brain Bank under the original donor consent procedures; the GSE136666 study identifies NBB Project 870 [27,28]. The source publication for GSE243639 reports Ethics Committee approval at UZ Leuven/KU Leuven under S64182 [29]. The present work reanalyzed de-identified deposited data without recruiting participants or collecting tissue.

Informed Consent Statement: Written informed consent was obtained in the original PPMI study. The Netherlands Brain Bank studies report donor consent for autopsy and research use of tissue and clinical information [27,28]. GSE243639 was generated under the original study's ethical approvals and consent procedures [29]. This secondary analysis reports no identifiable participant information.

Data Availability Statement: Participant-level clinical and metabolomic data were obtained from the Parkinson's Progression Markers Initiative (PPMI) and require authorization through PPMI under its access and data-use terms. Public transcriptomic data are available in the Gene Expression Omnibus under GSE168496, GSE136666, and GSE243639. Essential methods and results are reported in this article and its appendices. Complete derived study results are available from the corresponding authors on reasonable request, subject to applicable privacy and data-use requirements. Code Availability: Analysis code, the data dictionary, and supporting instructions are available from the corresponding authors on reasonable request. Access to any associated participant-derived materials is subject to applicable privacy protections and PPMI data-use requirements.

Acknowledgments: Data used in this study were obtained from the Parkinson's Progression Markers Initiative (PPMI). PPMI is a public–private partnership funded by The Michael J. Fox Foundation for Parkinson's Research and its funding partners. The authors thank the PPMI investigators, study staff, participants, and their families for their contributions to the study. The authors also acknowledge the investigators who generated and made publicly available the transcriptomic datasets GSE168496, GSE136666, and GSE243639. During preparation of this manuscript, ChatGPT 5.6 Sol (OPENAI) was solely used to assist with language editing. The authors are responsible for the content, interpretation, and final manuscript.

Conflicts of Interest: The authors declare no conflicts of interest.

Abbreviations

BH, Benjamini–Hochberg; BMP, bis(monoacylglycerol) phosphate; CI, confidence interval; CSF, cerebrospinal fluid; FDR, false discovery rate; GEE, generalized estimating equations; GEO, Gene Expression Omnibus; IQR, interquartile range; KEGG, Kyoto Encyclopedia of Genes and Genomes; MDS-UPDRS, Movement Disorder Society-sponsored revision of the Unified Parkinson's Disease Rating Scale; MSigDB, Molecular Signatures Database; NES, normalized enrichment score; PCA, principal component analysis; PC1, principal component 1; PD, Parkinson's disease; PE, phosphatidylethanolamine; PIGD, postural instability and gait difficulty; PPMI, Parkinson's Progression Markers Initiative; QC, quality control; SD, standard deviation; UMAP, uniform manifold approximation and projection.

Appendix A. Participant Selection and Assay Information

The paired reference population comprised 213 participants. Sequential clinical-event selection began with 3367 candidate events; 1080 lacked an eligible untreated/OFF examination, 630 had incomplete PIGD items, one had incoherent component timing, 491 preceded the clinical index month and 13 were index-only events from participants without eligible post-index follow-up. The resulting longitudinal dataset contained 1152 observations from 193 participants. Figure A1 summarizes participant selection and score construction.

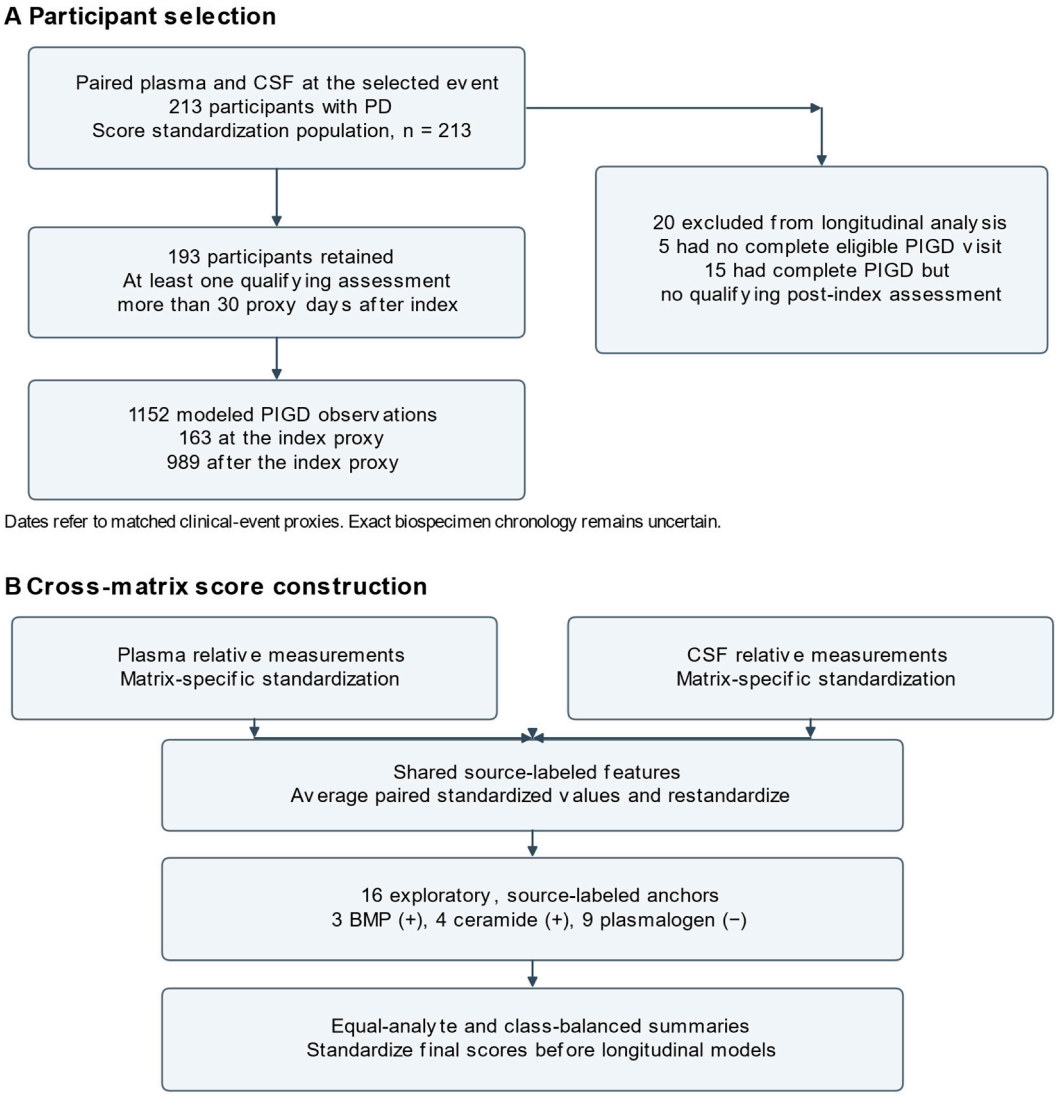


Figure A1. Participant selection and paired lipid-score construction. (**A**) Paired plasma and CSF measurements in 213 participants defined the standardization population. Five participants lacked a complete eligible PIGD assessment and 15 lacked eligible post-index follow-up, leaving 193 participants with 1152 observations (163 at index and 989 after index). (**B**) Within-matrix standardization, paired-feature averaging, restandardization and directional coding produced the equal-analyte and class-balanced scores. Directions describe the coding rule.

Project 180 data were identified by the provider's project and matrix fields. The plasma export comprised five parts; adjusted area ratios were present in part 5 and the CSF export, whereas plasma parts 1–4 contained area measurements. The provider's protocol, "LC/MS analysis of Plasma and CSF samples from PPMI" (Version 3, August 2024), describes both matrices and eight analytical batches per matrix. Participant-level analytical batch labels were unavailable for further adjustment. The analyzed export labels ended in 20 September 2026; provider update stamps were February/June 2022 for plasma and September 2024 for CSF. An independently recorded download date was unavailable.

Plasma and CSF were linked by participant and clinical-event identifier. Recorded clinical assessment months defined the time origin and follow-up axis. These source records did not resolve exact specimen collection dates or the plasma–CSF collection interval. The stricter same-month sensitivity analysis used 193 participants and 1149 observations.

Lipid names follow the provider's reported annotations and the protocol's targeted LC–MS/MS measurements. The secondary data did not provide additional orthogonal

confirmation of BMP versus phosphatidylglycerol isomers or plasmalogen linkage and positional specificity. The panel therefore retains the annotation resolution reported by the provider.

Appendix B. Transcriptomic Models and Pathway Analyses

Table A1 summarizes the experimental units and model specifications. Continuous covariates were standardized. Count-based differential expression used PyDESeq2 0.5.4, with median-of-ratios normalization and no prior log transformation; enrichment used GSEApy 1.3.1. Gene-level Benjamini–Hochberg adjustment was performed within each model.

Table A1. Transcriptomic experimental units and primary models.

Dataset and Tissue	PD/Control Units	Retained Genes	Primary Model
GSE168496, substantia nigra	8/8 donors	17,994	Sex + condition
GSE136666, substantia nigra	5/5 pools	22,280	Condition
GSE136666, putamen	3/3 pools	22,402	Condition
GSE243639, Astro pseudobulk	15/14 donors	16,785	Age + sex + PMI + RIN + condition

GSE136666 pools contained two donors per substantia nigra pool and three donors per putamen pool. Filtering required at least 10 counts in three samples for GSE168496, three substantia nigra pools or two putamen pools for GSE136666, and five donors for GSE243639. PMI, post-mortem interval; RIN, RNA integrity number.

For GSE168496, sex-adjusted models were supplemented separately by age or PMI. GSE136666 regional analyses included sex-adjusted models and exclusion of the QC-flagged pools GSM4054769 and GSM4054776. The Netherlands Brain Bank deposits lacked constituent identifiers needed to resolve donor overlap. GSE243639 sensitivities added a resequencing indicator or excluded Astro__D002. The Astro pseudobulk analysis comprised 20,710 nuclei; descriptive UMAP coordinates covered 16,322 nuclei. Counts per donor ranged from 174 to 1830 (median, 711), and age, sex, PMI, and RIN were complete.

Preranked enrichment used the signed PD-versus-control Wald statistic, weight 1, 10,000 permutations, and gene sets with 15–500 overlapping genes. Dataset seeds were 168496, 136666, and 243639. Symbols were uppercased, and duplicates were represented by the gene with the highest mean normalized abundance, with deterministic identifier tie-breaking. Non-finite statistics or raw *p*-values were excluded. Permutation-based FDR q-values were calculated within each full eligible library and model before selecting the eight lipid pathways for display.

Exploratory cell-composition models used donor-level centered log-ratio abundances with age, sex, PMI, and RIN, HC3 standard errors, and Benjamini–Hochberg adjustment within annotation family. Broad cell-type and astrocyte-subcluster results were considered in interpreting tissue and subpopulation differences. Volcano plots display finite log2 fold changes and adjusted *p*-values between zero and one; missing adjusted *p*-values are omitted, and a true zero is floored for display only.

Table A2. Eligible pathways in each enrichment testing family.

Context	Hallmark 2020	KEGG 2021 Human	Reactome 2022
T1	50	301	1114
T2	50	301	1115
T3	50	301	1115
T4	50	302	1090
T5	50	299	1085

Table A2. *Cont.*

Context	Hallmark 2020	KEGG 2021 Human	Reactome 2022
T6	50	302	1086
T7	50	299	1085
T8	50	291	1015
T9	50	291	1015
T10	50	287	1006

T1–T3: GSE168496 substantia nigra, respectively sex, sex + age, and sex + PMI; T4–T5: GSE136666 substantia nigra and putamen condition models; T6–T7: corresponding QC-exclusion models; T8–T10: GSE243639 fully adjusted Astro, resequencing-adjusted and donor-QC-exclusion models. These are model contexts within the source cohorts.

Table A3. Lipid-pathway enrichment across all ten displayed and sensitivity contexts.

Pathway	Context	NES	FDR q
H1	T1	−2.286	0
H1	T2	−2.269	0
H1	T3	−1.917	0.000459
H1	T4	−1.761	0.00468
H1	T5	−1.768	0.00687
H1	T6	−1.897	0.000692
H1	T7	−2.023	0.000441
H1	T8	−2.189	0
H1	T9	−2.180	0
H1	T10	−2.267	8.12×10^{-5}
H2	T1	−1.870	0.000424
H2	T2	−1.791	0.00157
H2	T3	−1.530	0.0238
H2	T4	−1.181	0.236
H2	T5	−1.122	0.297
H2	T6	−1.153	0.231
H2	T7	−1.135	0.293
H2	T8	−1.110	0.374
H2	T9	−1.119	0.344
H2	T10	−1.120	0.307
K1	T1	−2.263	2.01×10^{-5}
K1	T2	−2.136	0.000154
K1	T3	−1.944	0.00214
K1	T4	−1.596	0.0302
K1	T5	−1.316	0.149
K1	T6	−1.734	0.0136
K1	T7	−1.923	0.0026
K1	T8	−1.947	0.00305
K1	T9	−1.807	0.0107
K1	T10	−1.926	0.00382
K2	T1	−1.893	0.00241
K2	T2	−1.762	0.00966
K2	T3	−1.813	0.00689
K2	T4	−1.444	0.0794
K2	T5	−1.996	0.0016
K2	T6	−1.229	0.26
K2	T7	−1.503	0.0599
K2	T8	−1.048	0.583
K2	T9	0.869	1
K2	T10	−1.036	0.559
K3	T1	−1.749	0.0102
K3	T2	−1.591	0.0387

Table A3. *Cont.*

Pathway	Context	NES	FDR q
K3	T3	−1.592	0.0397
K3	T4	−1.537	0.0445
K3	T5	−1.983	0.00173
K3	T6	−1.342	0.165
K3	T7	−1.577	0.0429
K3	T8	−1.601	0.0452
K3	T9	−1.239	0.287
K3	T10	−1.576	0.0431
R1	T1	−2.166	8.43×10^{-5}
R1	T2	−2.202	4.94×10^{-5}
R1	T3	−2.038	0.000841
R1	T4	−1.943	0.00261
R1	T5	−1.692	0.041
R1	T6	−1.780	0.00955
R1	T7	−1.982	0.00218
R1	T8	−1.739	0.025
R1	T9	−1.486	0.114
R1	T10	−1.738	0.0211
R2	T1	−2.009	0.000915
R2	T2	−2.038	0.000698
R2	T3	−1.749	0.0173
R2	T4	−1.430	0.118
R2	T5	−1.205	0.357
R2	T6	−1.615	0.0355
R2	T7	−1.442	0.117
R2	T8	−0.571	1
R2	T9	−0.902	0.784
R2	T10	−0.593	1
R3	T1	−1.882	0.00403
R3	T2	−1.860	0.00529
R3	T3	−1.809	0.0104
R3	T4	−1.486	0.0907
R3	T5	−1.283	0.266
R3	T6	−1.519	0.0646
R3	T7	−1.573	0.0551
R3	T8	−1.574	0.0711
R3	T9	−1.515	0.097
R3	T10	−1.596	0.056

H1, Hallmark Fatty Acid Metabolism; H2, Hallmark Bile Acid Metabolism; K1, KEGG Fatty Acid Degradation; K2, KEGG Biosynthesis of Unsaturated Fatty Acids; K3, KEGG Fatty Acid Elongation; R1, Reactome Mitochondrial Fatty Acid Beta-Oxidation; R2, Reactome Peroxisomal Lipid Metabolism; R3, Reactome Fatty Acid Metabolism. Negative NES indicates lower pathway transcription in PD. Zero q-values are empirical permutation estimates. Context definitions are given below Table A2.

None of the 31 donor-level composition components met their within-family BH threshold. The broad cell-type and partially annotated astrocyte-subcluster analyses were interpreted alongside the donor-level expression models. Excluding the flagged GSE136666 substantia nigra pool changed gene-level FDR findings from 178 to 473, with 158 shared findings; 90 of 95 metabolic-domain pathway rows retained their NES direction, and 39 met the FDR threshold in both analyses.

The complete gene-level comparisons, full-library pathway results, exact gene-set definitions and additional analytical documentation are available from the corresponding authors on reasonable request. Public source data remain accessible under the GEO accession numbers in the Data Availability Statement.

Appendix C. Additional Longitudinal Model Results

The reference model converged without warnings; random-intercept and residual variances were 0.15690 and 0.10666. The clinically adjusted model converged with random-intercept variance 0.04291 and residual variance 0.09030; a singular-covariance warning occurred during optimization despite the positive final variance. The random-slope reference fit converged with a variance-boundary warning: intercept variance 0.07571, slope variance 0.00961, intercept–slope covariance 0.01218, and residual variance 0.07039. Zero PIGD values occurred in 144/1152 assessments (12.5%), with no ceiling values. Reference residual skewness was 1.16, and the Spearman correlation between absolute residuals and fitted values was 0.385. These findings qualify the constant-variance Gaussian working model.

Each participant bootstrap used 1000 valid resamples, relabeled repeated sampled clusters, and held score construction and standardization fixed. Percentile 95% intervals were −0.00575–0.02503 for the reference association and −0.00241–0.02950 after clinical adjustment. Thus, both included zero. In the age/sex-by-time robust GEE, all 193 participant-deletion fits succeeded without sign reversal; estimates ranged from 0.00899 to 0.01497. The largest absolute deletion change was 0.603 of the full-model standard error. Influence stability does not resolve the post hoc selection or inference-method uncertainty.

In the same 193 participants and 1152 observations, class-balanced plasma-only and CSF-only estimates were 0.01309 (model-based 95% CI, 0.00486–0.02131) and 0.00770 (−0.00110–0.01649), respectively, compared with 0.01438 (0.00599–0.02278) for the integrated score. Additional BMI adjustment yielded an equal-analyte estimate of 0.00979 (0.00120–0.01839; 150 participants, 982 observations). Including visit-level dopaminergic-treatment status yielded 0.01425 (0.00664–0.02185; 162 participants, 1056 observations). In the quadratic-time model, the first-order score-by-time coefficient was 0.00910 (−0.01246–0.03066; 193 participants, 1152 observations). All estimates are annual PIGD differences per SD.

Follow-up reached 0, 1, 2, 3, 4, 5, 7, 10 and 12 years for 193, 182, 165, 148, 131, 105, 60, 13 and two participants, respectively. The annual retention-weighted sensitivity used probability bounds of 0.02–0.98 and weights truncated at the 1st and 99th percentiles (approximately 0.518–2.015); participant effective sample size was 174.90. Model specifications are described in Section 2.6. These estimates assess sensitivity to measured retention differences.

Table A4. Complete fixed-effect coefficients for the reference equal-analyte mixed model.

Term	Estimate	95% CI	*p*
Intercept	0.43889	0.34580–0.53199	2.46×10^{-20}
Sex (male vs. female)	−0.10658	−0.22820–0.01503	0.0859
Time (years)	0.06967	0.06168–0.07766	1.71×10^{-65}
Lipid score (SD)	0.03176	−0.03195–0.09546	0.329
Time × Lipid score (SD)	0.01248	0.00447–0.02048	0.00225
Age (centered years)	0.01035	0.00279–0.01791	0.00732

193 participants; 1152 observations. The outcome is the five-item PIGD mean (0–4). Time is measured in years; the lipid score is standardized to one SD. Age is centered. The score-by-time coefficient is the annual difference in PIGD change per SD. Intervals and *p*-values are model-based; the participant-bootstrap interval is reported separately. Sex was coded 0 for female and 1 for male. Index dopaminergic treatment was coded 0 for no and 1 for yes; treated participants contributed eligible OFF examinations.

Table A5. Complete fixed-effect coefficients for the clinically adjusted equal-analyte mixed model.

Term	Estimate	95% CI	*p*
Intercept	−0.01997	−0.15745–0.11750	0.776
Sex (male vs. female)	−0.01605	−0.10589–0.07380	0.726
Time (years)	0.05442	0.03062–0.07822	7.42×10^{-6}
Time × Sex (male vs. female)	0.00444	−0.01200–0.02088	0.596
Lipid score (SD)	0.00977	−0.03294–0.05247	0.654
Age (centered years)	−0.00016	−0.00540–0.00507	0.951
Disease duration (years)	0.01304	−0.01173–0.03781	0.302
Index PIGD	0.99761	0.83674–1.15848	5.43×10^{-34}
Index Part III, non-gait	0.00012	−0.00419–0.00444	0.956
Index treatment (yes vs. no)	−0.02840	−0.12757–0.07076	0.575
LRRK2 carrier indicator	0.00385	−0.09659–0.10429	0.94
GBA carrier indicator	−0.03188	−0.17607–0.11232	0.665
Time × Lipid score (SD)	0.01408	0.00646–0.02170	0.000291
Time × Age (centered years)	0.00299	0.00205–0.00393	5.4×10^{-10}
Time × Disease duration (years)	0.00286	−0.00174–0.00747	0.223
Time × Index PIGD	−0.02516	−0.05975–0.00943	0.154
Time × Index Part III, non-gait	0.00052	−0.00024–0.00128	0.179
Time × Index treatment (yes vs. no)	0.00843	−0.00880–0.02565	0.338
Time × LRRK2 carrier indicator	−0.01017	−0.02861–0.00826	0.279
Time × GBA carrier indicator	0.00197	−0.02927–0.03321	0.902

162 participants; 1056 observations, including index outcomes. All listed covariates also enter as interactions with time. Non-gait Part III excludes NP3GAIT, NP3FRZGT, and NP3PSTBL. Treatment and carrier variables are the recorded binary indicators. Intervals and *p*-values are model-based; bootstrap uncertainty is reported separately. Sex was coded 0 for female and 1 for male. Index dopaminergic treatment was coded 0 for no and 1 for yes; treated participants contributed eligible OFF examinations.

Table A6. Clinically adjusted five-score sensitivity families.

Score/Model	Annual β (95% CI)	*p*	BH q
Mixed effects			
Equal-analyte	0.01408 (0.00646–0.02170)	0.000291	0.000727
Class-balanced	0.01612 (0.00802–0.02423)	9.71×10^{-5}	0.000486
BMP–ceramide	0.00642 (−0.00113–0.01396)	0.0956	0.119
Plasmalogen-deficit	0.00628 (−0.00099–0.01356)	0.0906	0.119
PC1 (110 features)	−0.00194 (−0.00904–0.00515)	0.591	0.591
Robust GEE			
Equal-analyte	0.01402 (0.00168–0.02636)	0.0259	0.0648
Class-balanced	0.01630 (0.00385–0.02874)	0.0103	0.0514
BMP–ceramide	0.00662 (−0.00444–0.01768)	0.241	0.401
Plasmalogen-deficit	0.00615 (−0.00717–0.01948)	0.365	0.457
PC1 (110 features)	−0.00210 (−0.01511–0.01091)	0.751	0.751

Each specification uses 162 participants and 1056 observations. β is the score-by-time interaction per SD. Benjamini–Hochberg correction is applied separately to the five score tests within each specification. Mixed-model intervals are model based; GEE intervals use robust sandwich standard errors. No score reaches $q < 0.05$ in the clinically adjusted GEE family.

Complete model output, participant-bootstrap replicates and further derived analytical results are available from the corresponding authors on reasonable request, subject to applicable privacy and data-use requirements.

Table A7. Individual-anchor associations under the reference model.

Lipid Anchor	Annual β (95% CI)	*p*	BH q
BMP(18:0_18:1)	0.01353 (0.00512–0.02194)	0.00162	0.0259
BMP(18:1/18:1)	0.00610 (−0.00203–0.01423)	0.141	0.323
BMP(22:6/22:6)	0.00193 (−0.00670–0.01055)	0.661	0.914
Cer(d18:1/16:0)	−0.00134 (−0.00944–0.00677)	0.746	0.914
Cer(d18:1/18:0)	0.00049 (−0.00832–0.00929)	0.914	0.914
Cer(d18:1/24:0)	0.00264 (−0.00441–0.00968)	0.463	0.824
Cer(d18:1/24:1)	0.00606 (−0.00109–0.01320)	0.0966	0.296
PE(P-16:0/20:4)	−0.00087 (−0.00843–0.00669)	0.822	0.914
PE(P-16:0/22:4)	−0.01114 (−0.01885–−0.00344)	0.00459	0.0367
PE(P-16:0/22:6)	−0.00661 (−0.01453–0.00131)	0.102	0.296
PE(P-18:0/18:1)	−0.00067 (−0.00812–0.00677)	0.859	0.914
PE(P-18:0/18:2)	−0.00060 (−0.00830–0.00710)	0.878	0.914
PE(P-18:0/20:4)	−0.00073 (−0.00883–0.00737)	0.86	0.914
PE(P-18:0/22:6)	−0.01052 (−0.01858–−0.00245)	0.0106	0.0567
PE(P-18:1/20:4)	−0.00395 (−0.01182–0.00393)	0.326	0.652
PE(P-18:1/22:6)	−0.00646 (−0.01439–0.00148)	0.111	0.296

193 participants; 1152 observations. Each anchor is standardized and tested separately using the reference random-intercept specification. Effects retain their original abundance direction before the composite's sign coding; therefore, a negative plasmalogen coefficient is not inconsistent with a positive plasmalogen-deficit direction. BH q-values use the separate 16-anchor family. Provider analyte labels are retained.

Table A8. All 16 leave-one-anchor reference-model analyses.

Omitted Anchor	Annual β	95% CI	*p*
BMP(18:0_18:1)	0.01013	0.00225–0.01801	0.0118
BMP(18:1/18:1)	0.01114	0.00324–0.01903	0.00569
BMP(22:6/22:6)	0.01214	0.00413–0.02016	0.00299
Cer(d18:1/16:0)	0.01198	0.00417–0.01979	0.00264
Cer(d18:1/18:0)	0.01189	0.00400–0.01978	0.00314
Cer(d18:1/24:0)	0.01149	0.00350–0.01947	0.00482
Cer(d18:1/24:1)	0.01111	0.00310–0.01912	0.00658
PE(P-16:0/20:4)	0.01376	0.00580–0.02173	0.000709
PE(P-16:0/22:4)	0.01173	0.00350–0.01997	0.00523
PE(P-16:0/22:6)	0.01267	0.00458–0.02076	0.00214
PE(P-18:0/18:1)	0.01424	0.00608–0.02239	0.000621
PE(P-18:0/18:2)	0.01379	0.00573–0.02185	0.000796
PE(P-18:0/20:4)	0.01391	0.00595–0.02187	0.000611
PE(P-18:0/22:6)	0.01209	0.00397–0.02021	0.00352
PE(P-18:1/20:4)	0.01330	0.00530–0.02130	0.00112
PE(P-18:1/22:6)	0.01267	0.00458–0.02075	0.00214

193 participants; 1152 observations for each fit. After each deletion, the remaining 15-anchor equal-analyte score was reconstructed and standardized using the same weighting rule, then fitted with the reference random-intercept model. Intervals and *p*-values are model-based; deletion *p*-values are descriptive and are not a new confirmatory testing family. All 16 reference estimates are shown; alternative-covariance deletion results are available on request.

Table A9. Complete oriented PC1 loadings for the 110 shared lipid features.

Feature	Loading	Feature	Loading
(3-O-sulfo)GalCer(d18:1/16:0)	−0.09912	LPI(16:0)	−0.10532
(3-O-sulfo)GalCer(d18:1/18:0(2OH)	−0.08597	LPI(18:0)	−0.11521
(3-O-sulfo)GalCer(d18:1/18:0)	−0.11082	LacCer(d18:1/16:0)	−0.06522
(3-O-sulfo)GalCer(d18:1/24:0(2OH))	−0.09335	LacCer(d18:1/18:0)	−0.02254
(3-O-sulfo)GalCer(d18:1/24:0)	−0.07943	Oleic acid	−0.04901

Table A9. *Cont.*

Feature	Loading	Feature	Loading
(3-O-sulfo)GalCer(d18:1/24:1(2OH))	−0.10517	PA(16:0_18:1)	−0.07147
(3-O-sulfo)GalCer(d18:1/24:1)	−0.09662	PC(34:1)	−0.12487
7-alpha-Hydroxy-3-oxo-4-cholestenoate	−0.05785	PC(36:1)	−0.13664
Arachidonic acid_MRM	−0.10230	PC(36:2)	−0.11694
BMP(18:0_18:1)	−0.07872	PC(36:4)	−0.10867
BMP(18:1/18:1)	−0.09715	PC(38:4)	−0.11120
BMP(22:6/22:6)	−0.04572	PC(38:6)	−0.10133
CE(16:1)	−0.09638	PC(40:5)	−0.09367
CE(18:1)	−0.12462	PC(40:6)	−0.09757
CE(18:2)	−0.09162	PC(O-16:0/0:0)	−0.06334
CE(20:4)	−0.09739	PC(O-16:0/2:0)	−0.12013
CE(20:5)	−0.06668	PC(O-18:0/2:0)	−0.12180
CE(22:6)	−0.09405	PE(34:1)	−0.09308
Cer(d18:1/16:0)	−0.11046	PE(36:1)	−0.09015
Cer(d18:1/18:0)	−0.09648	PE(36:2)	−0.10132
Cer(d18:1/24:0)	−0.09786	PE(36:4)	−0.08890
Cer(d18:1/24:1)	−0.11269	PE(38:4)	−0.10228
Cholesterol	−0.10468	PE(38:5)	−0.09481
Cholesterol sulfate	−0.03217	PE(38:6)	−0.09236
DG(16:0_18:1)	−0.05476	PE(40:4)	−0.07603
DG(18:0_22:6)	−0.02592	PE(40:6)	−0.08169
DG(18:1/18:1)	−0.05171	PE(40:7)	−0.08392
DHA	−0.07746	PE(O-16:0/20:4)	−0.09714
Dimethylethanolamine	−0.02104	PE(O-16:0/22:6)	−0.10321
Ethanolamine	−0.05320	PE(O-18:0/20:4)	−0.10948
GD1a/b(d36:1)	−0.07573	PE(O-18:0/22:6)	−0.09265
GM3(d34:1)	−0.11445	PE(P-16:0/20:4)	−0.10417
GM3(d36:1)	−0.12020	PE(P-16:0/22:4)	−0.09635
GalCer(d18:1/16:0)	−0.09422	PE(P-16:0/22:6)	−0.10939
GalCer(d18:2/18:0)	−0.09701	PE(P-18:0/18:1)	−0.11422
GalCer(d18:2/20:0)	−0.08117	PE(P-18:0/18:2)	−0.08461
GlcCer(d18:1/16:0)	−0.10262	PE(P-18:0/20:4)	−0.11506
GlcCer(d18:1/18:0)	−0.10009	PE(P-18:0/22:6)	−0.10190
GlcCer(d18:1/22:0)	−0.07127	PE(P-18:1/20:4)	−0.11602
Glycerophosphocholine	−0.08927	PE(P-18:1/22:6)	−0.10402
HexCer(d18:1/16:0)	−0.09810	PG(16:0_18:1)	−0.08587
HexCer(d18:1/18:0)	−0.09828	PG(18:0_18:1)	−0.07579
HexCer(d18:1/22:0)	−0.08484	PI(16:0_18:1)	−0.09063
HexCer(d18:1/24:0)	−0.07849	PI(16:0_20:4)	−0.10593
HexCer(d18:1/24:1)	−0.08452	PI(18:0_18:1)	−0.08969
LPC(16:0)	−0.13025	PI(18:0_20:4)	−0.12657
LPC(16:1)	−0.11017	PI(18:0_22:6)	−0.08334
LPC(18:0)	−0.12868	PI(18:1/18:1)	−0.08461
LPC(18:1)	−0.12356	Palmitic acid	−0.01845
LPC(20:4)	−0.10824	SM(d18:1/16:0)	−0.13753
LPC(22:6)	−0.10239	SM(d18:1/18:0)	−0.12010
LPE(16:0)	−0.10747	SM(d18:1/24:0)	−0.11245
LPE(18:0)	−0.10851	SM(d18:1/24:1)	−0.12529
LPG(16:0)	−0.05836	TG(18:0_36:2)	−0.04141
LPG(18:1)	−0.06874	TG(18:1_34:2)	−0.04101

The PC1 comparator uses all 110 shared features in the 213-participant paired reference population and explains 33.66% of variance. Signs are oriented by alignment with the anchor-direction vector. Read down the left feature/loading pair, then the right pair. Provider feature identifiers, including their punctuation, are reproduced without structural reinterpretation. Values are rounded to five decimals; this table reports loadings, not clinical effects.

References

1. Hähnel, T.; Raschka, T.; Sapienza, S.; Klucken, J.; Glaab, E.; Corvol, J.C.; Falkenburger, B.H.; Fröhlich, H. Progression subtypes in Parkinson's disease identified by a data-driven multi cohort analysis. *npj Park. Dis.* **2024**, *10*, 95. [CrossRef]

2. Dadu, A.; Satone, V.; Kaur, R.; Hashemi, S.H.; Leonard, H.; Iwaki, H.; Makarious, M.B.; Billingsley, K.J.; Bandres-Ciga, S.; Sargent, L.J.; et al. Identification and prediction of Parkinson's disease subtypes and progression using machine learning in two cohorts. *npj Park. Dis.* **2022**, *8*, 172. [CrossRef]
3. Lian, J.; Luo, X.; Shan, C.; Han, D.; Zhang, C.; Vardhanabhuti, V.; Li, D.; Qiu, L. Personalized progression modelling and prediction in Parkinson's disease with a novel multi-modal graph approach. *npj Park. Dis.* **2024**, *10*, 229. [CrossRef]
4. Stebbins, G.T.; Goetz, C.G.; Burn, D.J.; Jankovic, J.; Khoo, T.K.; Tilley, B.C. How to identify tremor dominant and postural instability/gait difficulty groups with the movement disorder society unified Parkinson's disease rating scale: Comparison with the unified Parkinson's disease rating scale. *Mov. Disord.* **2013**, *28*, 668–670. [CrossRef]
5. Li, Y.; Huang, X.; Ruan, X.; Duan, D.; Zhang, Y.; Yu, S.; Chen, A.; Wang, Z.; Zou, Y.; Xia, M.; et al. Baseline cerebral structural morphology predict freezing of gait in early drug-naïve Parkinson's disease. *npj Park. Dis.* **2022**, *8*, 176. [CrossRef]
6. Sarasso, E.; Basaia, S.; Cividini, C.; Stojkovic, T.; Stankovic, I.; Piramide, N.; Tomic, A.; Markovic, V.; Stefanova, E.; Kostic, V.S.; et al. MRI biomarkers of freezing of gait development in Parkinson's disease. *npj Park. Dis.* **2022**, *8*, 158. [CrossRef]
7. Herman, T.; Barer, Y.; Bitan, M.; Sobol, S.; Giladi, N.; Hausdorff, J.M. A meta-analysis identifies factors predicting the future development of freezing of gait in Parkinson's disease. *npj Park. Dis.* **2023**, *9*, 158. [CrossRef]
8. Mirelman, A.; Volkov, J.; Salomon, A.; Gazit, E.; Nieuwboer, A.; Rochester, L.; Del Din, S.; Avanzino, L.; Pelosin, E.; Bloem, B.R.; et al. Digital Mobility Measures: A Window into Real-World Severity and Progression of Parkinson's Disease. *Mov. Disord.* **2024**, *39*, 328–338. [CrossRef]
9. Shahmoradian, S.H.; Lewis, A.J.; Genoud, C.; Hench, J.; Moors, T.E.; Navarro, P.P.; Castaño-Díez, D.; Schweighauser, G.; Graff-Meyer, A.; Goldie, K.N.; et al. Lewy pathology in Parkinson's disease consists of crowded organelles and lipid membranes. *Nat. Neurosci.* **2019**, *22*, 1099–1109. [CrossRef]
10. Galper, J.; Dean, N.J.; Pickford, R.; Lewis, S.J.G.; Halliday, G.M.; Kim, W.S.; Dzamko, N. Lipid pathway dysfunction is prevalent in patients with Parkinson's disease. *Brain* **2022**, *145*, 3472–3487. [CrossRef]
11. Merchant, K.M.; Simuni, T.; Fedler, J.; Caspell-Garcia, C.; Brumm, M.; Nudelman, K.N.H.; Tengstrandt, E.; Hsieh, F.; Alcalay, R.N.; Coffey, C.; et al. LRRK2 and GBA1 variant carriers have higher urinary bis(monacylglycerol) phosphate concentrations in PPMI cohorts. *npj Park. Dis.* **2023**, *9*, 30. [CrossRef]
12. Medoh, U.N.; Abu-Remaileh, M. The Bis(monoacylglycero)-phosphate Hypothesis: From Lysosomal Function to Therapeutic Avenues. *Annu. Rev. Biochem.* **2024**, *93*, 447–469. [CrossRef]
13. Hällqvist, J.; Toomey, C.E.; Pinto, R.; Baldwin, T.; Doykov, I.; Wernick, A.; Al Shahrani, M.; Evans, J.R.; Lachica, J.; Pope, S.; et al. Multi-omic analysis reveals lipid dysregulation associated with mitochondrial dysfunction in parkinson's disease brain. *Nat. Commun.* **2025**, *16*, 10490. [CrossRef]
14. Yilmaz, A.; Ashrafi, N.; Ashrafi, R.; Akyol, S.; Saiyed, N.; Kerševičiūtė, I.; Gabrielaite, M.; Gordevicius, J.; Graham, S.F. Lipid profiling of Parkinson's disease brain highlights disruption in Lysophosphatidylcholines, and triacylglycerol metabolism. *npj Park. Dis.* **2025**, *11*, 159. [CrossRef]
15. Galper, J.; Mori, G.; McDonald, G.; Ahmadi Rastegar, D.; Pickford, R.; Lewis, S.J.G.; Halliday, G.M.; Kim, W.S.; Dzamko, N. Prediction of motor and non-motor Parkinson's disease symptoms using serum lipidomics and machine learning: A 2-year study. *npj Park. Dis.* **2024**, *10*, 123. [CrossRef]
16. Paul, K.C.; Zhang, K.; Walker, D.I.; Sinsheimer, J.; Yu, Y.; Kusters, C.; Del Rosario, I.; Folle, A.D.; Keener, A.M.; Bronstein, J.; et al. Untargeted serum metabolomics reveals novel metabolite associations and disruptions in amino acid and lipid metabolism in Parkinson's disease. *Mol. Neurodegener.* **2023**, *18*, 100. [CrossRef]
17. Li, Y.; Ji, G.; Lian, M.; Liu, X.; Xu, Y.; Gui, Y. Effect of PLA2G6 and SMPD1 Variants on the Lipid Metabolism in the Cerebrospinal Fluid of Patients with Parkinson's Disease: A Non-targeted Lipidomics Study. *Neurol. Ther.* **2023**, *12*, 2021–2040. [CrossRef]
18. Flores-Torres, M.H.; Peng, X.; Jeanfavre, S.; Clish, C.; Wang, Y.; McCullough, M.L.; Healy, B.; Schwarzschild, M.A.; Bjornevik, K.; Ascherio, A. Plasma Metabolomics Profiles in Prodromal and Clinical Parkinson's Disease. *Mov. Disord.* **2025**, *40*, 2209–2219. [CrossRef]
19. Gervasoni, J.; Marino, C.; Imarisio, A.; Santucci, L.; Napolitano, E.; Nuzzo, T.; Yahyavi, I.; Avenali, M.; Cicchinelli, M.; Buongarzone, G.; et al. Independent serum metabolomics approaches identify disrupted glutamic acid and serine metabolism in Parkinson's disease patients. *npj Park. Dis.* **2025**, *11*, 274. [CrossRef]
20. Smajić, S.; Prada-Medina, C.A.; Landoulsi, Z.; Ghelfi, J.; Delcambre, S.; Dietrich, C.; Jarazo, J.; Henck, J.; Balachandran, S.; Pachchek, S.; et al. Single-cell sequencing of human midbrain reveals glial activation and a Parkinson-specific neuronal state. *Brain* **2022**, *145*, 964–978. [CrossRef]
21. Basurco, L.; Abellanas, M.A.; Ayerra, L.; Conde, E.; Vinueza-Gavilanes, R.; Luquin, E.; Vales, A.; Vilas, A.; Martin-Uriz, P.S.; Tamayo, I.; et al. Microglia and astrocyte activation is region-dependent in the α-synuclein mouse model of Parkinson's disease. *Glia* **2023**, *71*, 571–587. [CrossRef]
22. Liu, Y.; Cao, L.; Song, Y.; Kang, Z.; Liu, T.; Ding, J.; Hu, G.; Lu, M. Mitochondrial glutamine transporter SLC1A5_var, a potential target to suppress astrocyte reactivity in Parkinson's Disease. *Cell Death Dis.* **2022**, *13*, 946. [CrossRef]

23. Chi, X.; Yin, S.; Sun, Y.; Kou, L.; Zou, W.; Wang, Y.; Jin, Z.; Wang, T.; Xia, Y. Astrocyte-neuron communication through the complement C3-C3aR pathway in Parkinson's disease. *Brain Behav. Immun.* **2025**, *123*, 229–243. [CrossRef]
24. Wang, P.; Lan, G.; Xu, B.; Yu, Z.; Tian, C.; Lei, X.; Meissner, W.G.; Feng, T.; Yang, Y.; Zhang, J. α-Synuclein-carrying astrocytic extracellular vesicles in Parkinson pathogenesis and diagnosis. *Transl. Neurodegener.* **2023**, *12*, 40. [CrossRef]
25. Marek, K.; Jennings, D.; Lasch, S.; Siderowf, A.; Tanner, C.; Simuni, T.; Coffey, C.; Kieburtz, K.; Flagg, E.; Chowdhury, S.; et al. The Parkinson Progression Marker Initiative (PPMI). *Prog. Neurobiol.* **2011**, *95*, 629–635. [CrossRef]
26. Benjamini, Y.; Hochberg, Y. Controlling the False Discovery Rate: A Practical and Powerful Approach to Multiple Testing. *J. R. Stat. Soc. Ser. B Methodol.* **1995**, *57*, 289–300. [CrossRef]
27. Tranchevent, L.-C.; Halder, R.; Glaab, E. Systems level analysis of sex-dependent gene expression changes in Parkinson's disease. *npj Park. Dis.* **2023**, *9*, 8. [CrossRef]
28. Xicoy, H.; Brouwers, J.F.; Wieringa, B.; Martens, G.J.M. Explorative Combined Lipid and Transcriptomic Profiling of Substantia Nigra and Putamen in Parkinson's Disease. *Cells* **2020**, *9*, 1966. [CrossRef]
29. Martirosyan, A.; Ansari, R.; Pestana, F.; Hebestreit, K.; Gasparyan, H.; Aleksanyan, R.; Hnatova, S.; Poovathingal, S.; Marneffe, C.; Thal, D.R.; et al. Unravelling cell type-specific responses to Parkinson's Disease at single cell resolution. *Mol. Neurodegener.* **2024**, *19*, 7. Correction in *Mol. Neurodegener.* **2024**, *19*, 28. [CrossRef]
30. Love, M.I.; Huber, W.; Anders, S. Moderated estimation of fold change and dispersion for RNA-seq data with DESeq2. *Genome Biol.* **2014**, *15*, 550. [CrossRef]
31. Subramanian, A.; Tamayo, P.; Mootha, V.K.; Mukherjee, S.; Ebert, B.L.; Gillette, M.A.; Paulovich, A.; Pomeroy, S.L.; Golub, T.R.; Lander, E.S.; et al. Gene set enrichment analysis: A knowledge-based approach for interpreting genome-wide expression profiles. *Proc. Natl. Acad. Sci. USA* **2005**, *102*, 15545–15550. [CrossRef]

Disclaimer/Publisher's Note: The statements, opinions and data contained in all publications are solely those of the individual author(s) and contributor(s) and not of MDPI and/or the editor(s). MDPI and/or the editor(s) disclaim responsibility for any injury to people or property resulting from any ideas, methods, instructions or products referred to in the content.